OXIDACIÓN FOTOELETROQUÍMICA DE FENOL EN SOLUCIÓN ACUOSA MEDIANTE EL USO DE PELÍCULAS DE TiO_2 DOPADAS CON BORO/GRAFENO INMOVILIZADAS SOBRE ACERO INOXIDABLE

ANDRÉS FABIÁN GUALDRÓN REYES

UNIVERSIDAD INDUSTRIAL DE SANTANDER

FACULTAD DE CIENCIAS

ESCUELA DE QUÍMICA

CENTRO DE MATERIALES Y NANOCIENCIAS – CMN

CENTRO DE INVESTIGACIONES EN CATÁLISIS – CICAT

BUCARAMANGA

2014

OXIDACIÓN FOTOELETROQUÍMICA DE FENOL EN SOLUCIÓN ACUOSA MEDIANTE EL USO DE PELÍCULAS DE TiO_2 DOPADAS CON BORO/GRAFENO INMOVILIZADAS SOBRE ACERO INOXIDABLE

ANDRÉS FABIÁN GUALDRÓN REYES

Trabajo de grado presentado como requisito

Para optar al título de Magister en Química

Directores

Dra. MARTHA EUGENIA NIÑO GÓMEZ

Dr. ÁNGEL MANUEL MELÉNDEZ REYES

UNIVERSIDAD INDUSTRIAL DE SANTANDER

FACULTAD DE CIENCIAS

ESCUELA DE QUÍMICA

CENTRO DE MATERIALES Y NANOCIENCIAS – CMN

CENTRO DE INVESTIGACIONES EN CATÁLISIS – CICAT

BUCARAMANGA

2014

Dedicatoria

A Normelis, Venancio y Daniela

Por ser mi fuerza y motivación diaria para

Alcanzar mis objetivos; a Jessyka por sus sabios consejos,

Paciencia y cariño incondicional,

Y a mis amigos por su apoyo.

Agradecimientos

Al centro de Materiales y Nanociencias (CMN) Laboratorio 304S y el Centro de Investigaciones en Catálisis (CICAT) por la infraestructura proporcionada para la realización del trabajo.

A los profesores Ángel Manuel Meléndez y Martha Eugenia Niño por sus consejos antes, durante y posterior a la culminación del trabajo, así como su gran entrega como “padres académicos” para mi crecimiento personal y profesional.

A la Universidad Autónoma Metropolitana UAM-I Laboratorio de Electroquímica y en especial al profe Ignacio González por asesorarme durante mi estancia internacional. Y no me olvido de Msc. Edgar Carrera, quien tuvo paciencia a mis preguntas un tanto salidas de contexto. Al profesor Luis Lartundo Rojas por el análisis XPS.

A María Isabel Carreño, Carlos Hernández, Linney, Jose Luis y demás chicos del CICAT y del LAB. 304 que de forma alternada a mi trabajo, ayudaron a complementar los principios básicos para la conformación de un gran grupo de investigación en este campo realmente importante como lo es la Electroquímica.

A mis amigos Jerfferson y Fernando, que me acompañaron desde mis primeros pinos en el pregrado y demás personas que de una u otra forma colaboraron a que mi desempeño profesional creciera de forma acelerada. A todo ellos les estaré eternamente agradecido.

A mis familiares que de siempre supieron que lo podría lograr… y a ti Jessyka María por inculcar orden y orientación en mi vida, visualizando un futuro cada vez más cerca.

TABLE DE CONTENIDO

LISTA DE TABLAS

Pag

LISTA DE FIGURAS

Pag

RESUMEN

TÍTULO: Oxidación fotoelectroquímica de fenol en solución acuosa mediante el uso de películas delgadas de TiO_2 dopadas con boro/grafeno inmovilizadas sobre acero inoxidable*****

AUTOR: GUALDRÓN REYES, Andrés Fabián******

PALABRAS CLAVES: TiO_2 dopado con boro, RGO, transporte electrónico, colector de corriente, fotocorriente, sustrato

El efecto del contenido de RGO en la fotocorriente generada en la oxidación de fenol bajo luz visible empleando películas compuestas de TiO_2 dopadas con boro/RGO depositadas sobre acero inoxidable 304 por el método sol-gel y la técnica dip-coating fue estudiado. Micrografías FESEM muestran películas fracturadas debido al estrés térmico en la fase de enfriamiento durante el proceso de calentamiento. Los resultados de GIXRD muestran que el boro está presente en las películas inhibiendo el crecimiento de los cristalitos. Espectros de DRS indican la formación de especies donadoras localizadas justo debajo de la banda de conducción (CB) del TiO2 tras el dopaje con boro. Estos estados fueron identificados mediante XPS. Voltamperogramas de barrido lineal muestran que la incorporación de RGO mejora el transporte de electrones fotogenerados dentro de las películas compuestas, incrementando la fotocorriente. Estos mejoramientos son explicados en la base de la habilidad de RGO para promover la separación de portadores de carga. El efecto del contenido de boro en la capacidad de fotogeneración de portadores de carga del TiO_2 también fue estudiado. La película compuesta con 0.03 wt% boro y 3 wt% de RGO exhibe la fotocorriente más alta la cual es 30 veces más alta comparada con la del TiO2. El efecto del sustrato fue comparado soportando la mejor película sobre placas de Titanio. Esta película mostró ser más fotoelectroquímicamente activa en un tiempo prolongado que la película sobre acero inoxidable.

* Trabajo de Investigación

** Facultad de Ciencias, Escuela de Química. Directores: Dr. Martha Eugenia Niño Gómez, Dr. Ángel Manuel Meléndez.

ABSTRACT

TITLE: Photoelectrochemical phenol oxidation in aqueous solution by using boron-doped TiO_2/graphene films deposited on stainless steel*****

AUTHOR: GUALDRÓN REYES, Andrés Fabián******

KEYWORDS: boron-doped TiO_2, RGO, electron transport, current collector, photocurrent, substrate.

The effect of graphene (RGO) content on the photocurrent generated in the phenol oxidation under visible light using boron-doped TiO_2/RGO composite films deposited on 304 stainless steel plates by sol-gel method and dip-coating technique was studied. FESEM micrographs display cracked films due thermal stress in the cooling down stage during the heating process. GIXRD results show that boron is present in the films inhibiting the growth of crystallites. DRS spectra indicate the formation of donor species located below the bottom of conduction band (CB) of TiO_2 after boron doping. The donor states are associated to Ti^{3+} species detected by XPS. Linear voltammograms show that RGO incorporation improves the photogenerated electron transport within the composite films, increasing the photocurrent. These enhancements are explained on the basis of the ability of graphene in promoting the charge carrier separation by transferring the photogenerated electrons from the illuminated TiO_2 to the current collector. The effect of boron content on the charge carrier photogeneration capability of TiO_2 was also studied. The composite film with 0.03 wt% boron and 3 wt% graphene exhibits the highest photocurrent which is 30 times compared with the photocurrent of the TiO_2 film. The effect of substrate was compared depositing the best composite film on Titanium plates. This film showed more photoelectroactivity in a prolonged time than the composite film deposited on stainless steel.

* Reseach paper

** Faculty of Science, School of Chemistry. Advisers: Dr. Martha Eugenia Niño Gómez, Dr. Ángel Manuel Meléndez

GENERAL INTRODUCTION

The presence of phenol in resulting wastewaters from industrial processes has been a relevant topic due to the increase in the concentration of this highly recalcitrant organic compound in aquiferous zones at national level during recent years. This contamination has motivated to the research of new alternatives and the improvement of detoxification and disinfection techniques with a growing demand at industrial level. Actually, the photoelectrochemistry (PEC) is considered as an efficient strategy to the remotion of organic compounds dissolved in water, with the capability of oxide highly toxic pollutants, compared with other oxidation processes.

This promissory technology combines the photocatalytic (PC) and electrochemical processes with the advantage of employing semiconductor materials deposited in conducting substrates, which can absorb visible light to carry out the pollutant oxidation with high effectiveness. Due to the majority of semiconductors used in photoelectrochemical (PEC) processes not presents conducting properties, decreasing its PEC performance, the incorporation of some materials to improve these conducting properties and increase the PEC performance of the semiconductor is essential.

According with this description, the preparation boron-doped TiO_2/graphene composite films deposited on 304 stainless steel active to the visible light, with high conducting properties, employed in the PEC phenol oxidation was proposed. The phenol with a concentration value established for the wastewaters from the Colombian industries was oxidized using the composite films under an artificial visible light source. First of all, important parameters as the graphene and boron content were determinated to obtain the best PEC response in the phenol oxidation. As an additional contribution in the performed research, the effect of conducting substrate in the PEC activity of the composite films was studied by comparing the 304 stainless steel and titanium substrates.

CHAPTER 1: PHOTOELECTROCHEMICAL POLLUTANT OXIDATION USING TIO_2 BASED FILMS DEPOSITED IN CONDUCTING SUBSTRATES

Generalities

TiO_2 is one of the most studied semiconductors in the development of new materials for disinfection and detoxification process of pollutant in wastewaters, due to its well known photocatalytic properties, thermal and chemical stability, and low costs. Unfortunately, TiO_2 exhibits a large band of 3.2 eV and thus is only active to the UV light with a wavelength of 390 nm below, which occupies a small fraction (5 %) of solar energy. The limited UV light absorption results in a low activity of TiO_2 [1]. Therefore, many studies have been explored to narrow the band gap of TiO_2 and maximize the utilization of solar energy [2]. The most used approach is to dope TiO_2 with different elements including metal [3] and non-metal elements, especially N [4], P [5] and C [6], which extend the light absorption of the semiconductor to the visible region, representing an additional advantage in energetic terms. Di valentin et al [7] observed that adding electron donor atoms as N, C, B and F to the crystalline structure of TiO_2, its photoactivation in the visible region could be reached. Recently, the boron doping has been broadly researched due to this atom extend the light absorption to the visible region by the formation of energy states within the band gap of TiO_2. When boron is incorporated to the TiO_2 lattice, it occupies interstitial positions, inducing the formation of Ti^{3+} donor states just below the bottom of conduction band (CB) of TiO_2 (at 1.58 eV below the bottom of CB). Thus, the material behaves a n-type semiconductor. The electrons are promoted from the valence band to these states, extending the light absorption to the visible region. Subsequently, the electrons are promoted from these states to the CB of TiO_2, inhibiting the charge carrier recombination. Hence, the visible light absorption capability of TiO_2 can be enhanced [7].

Many researchers have developed modified TiO_2 active to the visible light as powders to be employed in aqueous suspensions, but using the powder catalyst

has the disadvantages like stirring during the reaction and separation of catalyst after each run [8, 9]. The preparation of TiO_2 films overcomes these problems and it also extends the applications of catalyst towards antibacterial ceramic tiles as well as self-cleaning glasses [3]. Among the different thin film deposition techniques the sol–gel dip coating is the simplest, economical and has advantages such as TiO_2 is easily anchored on the substrates bearing the complicated shapes and large area substrates. The films are normally prepared from TiO_2 dispersions using titania P25 and polyethylene glycol as principal precursors. However, the films obtained from suspensions, present low adherence, promoting the detachment from the substrate 10]. Hence, TiO_2 films with high adherence can be obtained from sol solutions employing titanium butoxide and acetylacetone as principal precursors dissolved in some alcohols as ethanol or butanol [11].

The TiO_2 films deposited on conducting substrates are commonly used in photocatalytic (PC) processes. In these processes, a TiO_2 film is illuminated with an irradiation equal or higher energy to the band gap of the semiconductor, photogenerating the electron/hole pairs to carry out redox reactions [12]. However, the electron/hole pair recombination can hinder these processes, decreasing the oxidative capability of TiO_2. The photoelectrochemical (PEC) processes take advantage of the PC processes due to the applying a potential across the film. In the PEC process, when the TiO_2 film is illuminated, the electron/hole pairs are generated; holes are accumulated in the semiconductor while the electrons are transported from the TiO_2-electrolytic solution interfase through the film to reach the conducting substrate [13]. The electrons are transported through the external circuit of the PEC cell where are collected by a cathode, generating a photocurrent. Thus, the photogenerated electron/hole pair can be separated, inhibiting the charge carrier recombination.

Hence, the PEC process represents a technologic alternative for the remotion of organic pollutants dissolved in water, with high capability to oxide recalcitrant compounds as phenol, which has been an issue of environmental concern during

recent years due to its presence in resulting wastewaters from several industrial processes [14, 15]. The PC oxidation mechanism of phenol is well known, but a few works have reported about the PEC oxidation process. Yan Su et al [16] has been employed Si-doped TiO_2 films, indicating that the PEC phenol oxidation generates a photocurrent. In the PEC phenol oxidation using TiO_2 films can carry out by two forms: the first is denominated direct oxidation, where the holes accumulated in the semiconductor after the charge carrier separation (1), directly react with the adsorbed organic compounds in the film surface (2) [17].

$$TiO_2 \xrightarrow{h\nu} TiO_2 + h^+ + e^- \qquad (1)$$

$$TiO_2 + h^+ + R \rightarrow TiO_2 + RO + e^- \qquad (2)$$

The second is called indirect reaction, where the physisorbed H_2O molecules in the film surface react with the holes to promote the generation of highly oxidant species as the hydroxyl radicals (3). Subsequently, these radicals react with the organic compounds (4).

$$TiO_2 + H_2O + h^+ \rightarrow TiO_2[HO\cdot] + H^+ \qquad (3)$$

$$TiO_2[HO\cdot] + R \rightarrow TiO_2 + RO + H^+ + e^- \qquad (4)$$

Yang et al [17] has reported that both reactions can induce the formation of intermediates compounds e.g. hydroquinone, benzoquinone, catechol, etc. the mineralization of these compounds can be reached to obtain CO_2 and H_2O [17]. Thus, the PEC processes are a favourable alternative in the oxidation or degradation of organic compounds. However, the principal problem showed in the PEC process is the low conducting properties in materials as TiO_2, due to this material is a semiconductor. The tortuous way that the electrons must follow through the nanoparticles increases the probability of electron/hole pair recombination, restraining the electron transport within the film [13]. Thus, the PEC performance of the TiO_2 in oxidation processes can be limited by the electron

transport. One of the most attractive alternatives to resolve this problem is the incorporation of a material with high conducting properties as graphene.

Wang et al [10] have demonstrated that the incorporation of graphene in TiO_2 films increases the conductivity of the semiconductor, decreasing the photogenerated charge carrier recombination facilitating a less tortuous way for the electron transport from the TiO_2 film to the conducting substrate. This former can improve the PEC performance of the TiO_2

Therefore, in order to obtain TiO_2 films with high PEC properties for the pollutant oxidation under visible light illumination, the objectives described below were performed.

Objectives

General objective

Study the photoelectrochemical properties of the boron-doped TiO_2/graphene (B-TiO_2/RGO) composite films employed as photoanodes in the phenol oxidation under visible light.

Specific objectives

Prepare B-TiO_2/RGO composite films deposited on 304SS by the sol-gel dip-coating technique

Study the RGO and boron content on the increase of generated photocurrent by the B-TiO_2/RGO composite films in the photoelectrochemical phenol oxidation.

Characterize the morphological and physicochemical properties of the B-TiO_2/RGO composite film with the highest photoelectrochemical properties exhibited during the phenol oxidation.

References

[1] J. Yu, X. Zhao, Mater. Res. Bull. 35 (2000) 1293–1301.

[2] L. Deng, Y. Chen, M. Yao, S. Wang, B. Zhu, W. Huang, S. Zhang, Synthesis, characterization of B-doped TiO_2 nanotubes with high photocatalytic activity. J. Sol-Gel Sci. Technol. 53 (2010) 535–541

[3] R.S. Sonawane, B.B. Kale, M.K. Dongare, Preparation and photo-catalytic activity of Fe–TiO_2 thin films prepared by sol–gel dip coating. Mater. Chem. Phys. 85 (2004) 52–57.

[4]] G. Liu, X. Wang, L. Wang, Z. Chen, F. Li, G.Q. Lu, H.M. Cheng, Drastically enhanced photocatalytic activity in nitrogen doped mesoporous TiO_2 with abundant surface states. J. Colloid Interface Sci. 334 (2009) 171–17.

[5] Y. Lv, L. Yu, X. Zhang, J. Yao, R. Zou, Z. Dai, P-doped TiO_2 nanoparticles film coated on ground glass substrate and the repeated photodegradation of dye under solar light irradiation. Appl. Surf. Sci. 257 (2011) 5715–5719.

[6] L. C. Chen, Y. C. Ho, W.S. Guo, C.M. Huang, T.C. Pan, Enhanced visible light-induced photoelectrocatalytic degradation of phenol by carbon nanotube-doped TiO_2 electrodes. Electrochem. Acta 54 (2009) 3884–3891.

[7] C. Di Valentin, G. Pacchioni, Trends in non-metal doping of anatase TiO_2: B, C, N and F. Catal. Today 206 (2013) 12–18.

[8]L. Lopez, W. A. Daouda, D. Duttaa, B. C. Panther, T. W. Turney, Effect of substrate on surface morphology and photocatalysis of large-scale TiO_2 films. Appl. Surf. Sci. 265 (2013) 162-168.

[9] J. Yu, X. Zhao, Effect of substrates on the photocatalytic activity of nanometer TiO_2 thin films Mater. Res. Bull., 35 (2000) 1293–1301.

[10] P. Wang, Y. Ao, C. Wang, J. Hou, J. Qian, Enhanced photoelectrocatalytic activity for dye degradation by graphene–titania composite film electrodes. J. Hazard. Mater. 223–224 (2012) 79–83.

[11] S. Li, Q. Wang, T. Chen, Z. Zhou, Y. Wang, J. Fu,Study on cerium-doped nano-TiO_2 coatings for corrosion protection of 316 L stainless steel, Nanoscale Res. Lett. 7 (2012) 1–9.

[12] D. Chen, D. Yang, Q. Wang, Z. Jiang, Effects of Boron Doping on Photocatalytic Activity and Microstructure of Titanium Dioxide Nanoparticles. Ind. Eng. Chem. 45 (2006) 4110–4116.

[13] D. Wang, X. Li, J. Chen, X. Tao, Enhanced photoelectrocatalytic activity of reduced graphene oxide/TiO_2 composite films for dye degradation. Chem. Eng. J. 198–199 (2012) 547–554.

[14] J. Araña, E. PulidoMelián, V.M. Rodríguez López, A. Peña Alonso, A.M. Rodríguez, González, O. Díaz, J. Pérez Peña, Photocatalytic degradation of phenol and phenolic compounds. Part I. Adsorption and FTIR study. J. Hazar. Mater. 146 (2007) 520–528.

[15] E. Sirés, Remediation of water pollution caused by pharmaceutical residues based on electrochemical separation and degradation technologies: A review. Environ. Int. 40 (2012) 212.

[16] Y Su, S. Quan, X. Wu, S. Chen, Electrochemically assisted photocatalytic degradation of phenol using silicon-doped TiO_2nanofilm electrode. Desalin. 252 (2010) 143–148.

[17] J. Yang, J. Dai, C. Chen, J. Zhao, Effects of hydroxyl radicals and oxygen species on the 4-chlorophenol degradation by photoelectrocatalytic reactions with TiO_2-film electrodes, J. Photochem. Photobiol. A. 208 (2009) 66–77.

CHAPTER 2: PHOTOCURRENT IMPROVEMENT IN THE PHENOL OXIDATION UNDER VISIBLE LIGHT USING BORON-DOPED TIO_2/GRAPHENE COMPOSITE FILMS DEPOSITED ON 304 STAINLESS STEEL

Abstract

In this chapter, the effect of graphene content on the photocurrent generated in the phenol oxidation under visible light using boron-doped TiO_2/graphene composite films deposited on 304 stainless steel plates by sol-gel method and dip-coating technique is studied. The films were characterized by GIXRD, FESEM-EDS, DRS and XPS. Linear sweep voltammetry measurements show that graphene incorporation improves the photogenerated electron transport within the composite films, increasing the photocurrent. These enhancements are explained on the basis of the ability of graphene in promoting the charge carrier separation by transferring the photogenerated electrons from the illuminated TiO_2 to the current collector. The effect of boron content on the charge carrier photogeneration capability of TiO_2 is also studied. The composite film with 0.03 wt% boron and 3 wt% graphene exhibits the highest photocurrent which is 30 times compared with the TiO_2 film.

2.1 Introduction

In photoelectrochemical (PEC) and photovoltaic process, a photoanode composed by a nanoparticulated TiO_2 film is normally employed [1, 2]. When the film is illuminated, the electron/hole (e^-/h^+) pairs are generated. Holes are accumulated in the semiconductor while the electrons are transported from the TiO_2-electrolytic solution interfase through the film to reach the current collector, where the film is deposited [2]. Subsequently, the electrons are transported through the external circuit of the cell where are collected by a cathode, generating a photocurrent. However, when the TiO_2 films are obtained by the sol-gel method, the grain

boundaries form a high surface states density [3], limiting the charge collection. Furthermore, the tortuous way that the electrons must follow through the nanoparticles increase the probability of charge carriers (e^-/h^+) recombination, decreasing the generated photocurrent [3, 4].

Due to the diverse applications require an optimized charge transport, the enhancement of the electron transport within the TiO_2 films is essential. Many alternatives have been proposed to reach this objective such as the preparation of TiO_2 nanotubes to address the electron way [5], the combination of metal elements with TiO_2 based materials [6] or the use of composite metal oxides (e.g. core shell) with matched band gaps [7]. The reduced graphene oxide (RGO) is another alternative to improve the electron transport due to its unique attractive features such as a high specific surface area (approximately 2630 cm^2/g) and excellent electronic conductivity endowed by its π-π conjugation structure [4, 8]. The incorporation of RGO in TiO_2 (P25) nanoparticles has shown an improvement in the electron transport, increasing its PEC activity [3, 9]. However, these materials have been analyzed under UV illumination, limiting its PEC performance. Non-metal elements can incorporate in the TiO_2 films to extend the light absorption to the visible region and maximize the utilization of solar energy [10, 11]. On the other hand, although a few reports have displayed the positive role of RGO in TiO_2 films (TiO_2/RGO), the RGO incorporation only has been studied in films obtained from nanoparticles suspension, which can exhibit low adherence occasioning the detachment of the film from the current collector [3, 4]. The films preparation from the TiO_2 sol solutions can enhance the homogeneity and the adherence of the film on the current collector.

In this chapter, boron-doped TiO_2/RGO composite films (B-TiO_2/RGO) deposited on 304 stainless steel (304SS) plates were prepared by sol-gel method and dip-coating technique using B-TiO_2/RGO sol solutions. These materials were employed as photoanodes in a photoelectrochemical cell for the phenol oxidation under visible light illumination. Composite films were doped with boron due to this

element can shift the photoactivation to the visible region, which can increase the PEC performance of the composite films [12, 13]. The effectiveness of RGO to improve the photocurrent generation, increasing the electron transport within the TiO_2 films is presented.

2.2 Experimental section

2.2.1 Preparation of B-TiO_2/RGO composite films

All reagents were purchased from Sigma-Aldrich and Merck as shown in the table 1. RGO was synthesized and supplied by Vicente Rodríguez from Instituto Potosino de Investigación Científica y Tecnológica (IPICYT- México). This material was characterized in this section (See 2.2.2). Phenol was 99% analytical reagent grade. B-TiO_2/RGO sols with different boron and RGO content were prepared by sol-gel process dispersing 200 mg of RGO in 100 mL anhydrous ethanol by sonication in a Elma E 30H Elmasonic sonicator during 1 h to create 10 wt% RGO dispersion. Dispersions with 1 wt%, 2 wt%, 3 wt%, 4 wt% were prepared by diluting 10 wt% RGO dispersion in ethanol. A mixture of 3.5 mL of titanium butoxide and 1.0 mL of acetylacetone was added into each RGO dispersion under vigorous stirring at room temperature for 1 h. Then, boric acid was added in different weight ratios 0.1% wt, 0.2 wt % and 0.3 wt % (0.021 g, 0.035 g and 0.049 g). The corresponding weight ratio of added boron from boric acid in the sol solutions was 0.02 wt%, 0.03 wt% and 0.04 wt%.

304SS plates (20 mm x 40 mm x 2 mm) were ground with No. 120, 240, 320 and 600 emery papers. Plates were cleaned by sonication with ethanol and acetone. TiO_2 films with different boron and RGO content were deposited at a rate of 60 mm /min, followed by dehydration at 100°C for 10 min. The deposition and thermal treatment was repeated 3 times in order to prepare films with high adherence [17].

Films were calcined at 400°C with a constant heating rate of 3°C/min and hold for 90 min.

Table1. Employed reagents to the sol solution preparation

Reagent	Purchase	Purity (%)	Observation
Titanium butoxide (IV)	Aldrich	99.9%	Titanium precursor
Boric Acid	Aldrich	99.5%	Boron precursor
Acetylacetone	Aldrich	99.9%	Chelating agent
Ethanol	Merck		Solvent
Deionized water			σ=5.5 µS/m
RGO	IPICYT	-----	

2.2.2. Characterization of B-TiO_2/RGO composite films

First of all, the obtained RGO was studied by Raman spectroscopy using a Micro-Raman Horiba Jobin Yvon HR 320 spectrometer operated with a low-power green laser (150 W) equipped with a Olympus BX 40 attachement. The excitation wavelength was 532 nm. The Raman spectra were collected by means of back scattering geometry with an acquisition time of 50 seconds. The morphology of the composite films was analyzed by field emission scanning electron microscopy (FESEM) using a JOEL Quanta 650 FEG equipped with an EDAX Apollo X energy dispersive X-ray spectroscopy (EDS). The crystallinity of the materials was investigated with grazing incidence X-ray diffraction (GIXRD) in a Bruker D8 Discover diffractometer with Da Vinci geometry operated at 40 kV and 30 mA, using Cu Kα radiation (0.15406 nm) selected with Ni filter, in grazing incidence mode with a step of 0.015° and a counting time of 1.0 s per step.The analysis of the phases present in the composite film was analyzed by comparing the observed profile with the patterns reported in the PDF-2 database of the International Centre for Diffraction Data (ICDD). Diffuse reflectance spectra (DRS) were recorded with a

Shimadzu PC 2401 UV-Vis spectrophotometer. A 304SS plate was employed as a reference in the range of 200 – 800 nm. X-ray photoelectron spectroscopy (XPS) spectra were carried in aThermo Scientific K-alpha X-ray photoelectron spectrometer with an Al Kα X-ray source (1.487 eV). Carbon C 1speak is usually a good way to detect and compensate the charge shift effect. Unfortunately, carbon is not the main component of the film surfaces. Since oxygen is the predominant element in this type of films, O 1s peak is more suitable to detect and compensate the charge shift. Hence, the binding energy of XPS spectra was calibrated with reference to the O 1s peak (531 eV). Gaussian-Lorentzian mix function and Shirley background subtraction were employed to deconvolute the XPS Ti 2p, O 1s and C 1s spectra. Collected XPS spectra correspond to an average of three measurements in different points of each simple.

2.2.3 Photoelectrochemical measurements

Photoelectrochemical measurements for the B-TiO_2/RGO composite films were performed in a three-electrode cell with a potentiostat AUTOLAB PGSTAT 302N. A graphite rod was used as counter electrode (CE) and an Ag/AgCl (3M) as reference electrode (RE), respectively. The separation between the composite film and CE the was 2.0 cm, while the separation between the composite film and RE was 0.3 cm. Linear sweep voltammograms were obtained with a scan rate of $10mVs^{-1}$ using 0.1 M $HClO_4$ as supporting electrolyte, in presence and absence of 1 mM phenol with and without illumination. All the solutions were bubbled with nitrogen during 20 min to remove the dissolved oxygen. The visible light source was a 150 W metal halide lamp (MHN-TD Philips) with UV-block. To study the RGO content in the B-TiO_2/RGO composite films, boron content (0.02 wt %) was chosen to photoactive the films in the visible region. Subsequently, the boron content was also studied. The emission spectrum of the lamp is shown as supplementary material (Annex, Figure 1S). All the electrochemical experiments were performed at room temperature.

2.3 Results and discussion

2.3.1 RGO characterization

Figure 1 shows the corresponding Raman spectra of GO (Figure 1a) and RGO (Figure 1b) obtained after the chemical reduction employing hydrazine. Typically, two main bands exist in the spectra of graphene-based materials; the G band assigned to the presence of sp^2 carbon-type structure and the D band resulting from the structural imperfections created by the oxygen-containing groups on the carbon basal plane [15, 18]. The G peak positions are ~ 1592 cm^{-1} and 1573 cm^{-1} for GO and RGO, respectively. The red-shift can be attributed to the de-oxygenation of the GO after the reduction, which results in formation of more sp^2 carbon atoms [18]. On the other hand, the intensity ratio of D band to G band (I_D/I_G) of the GO is about 0.98, while for the RGO is 1.01.The increase of I_D/I_G ratio after reduction is commonly found in GO chemical reduction studies and it is caused by the decrease of average size of sp^2 domains after the reduction of GO, forming new sp^2 domains with smaller sizes than the ones present in GO before reduction, but are larger in quantities [18, 19].Hence, it can be suggest that after 1 h of hydrazine-reduction of GO, RGO can be obtained.

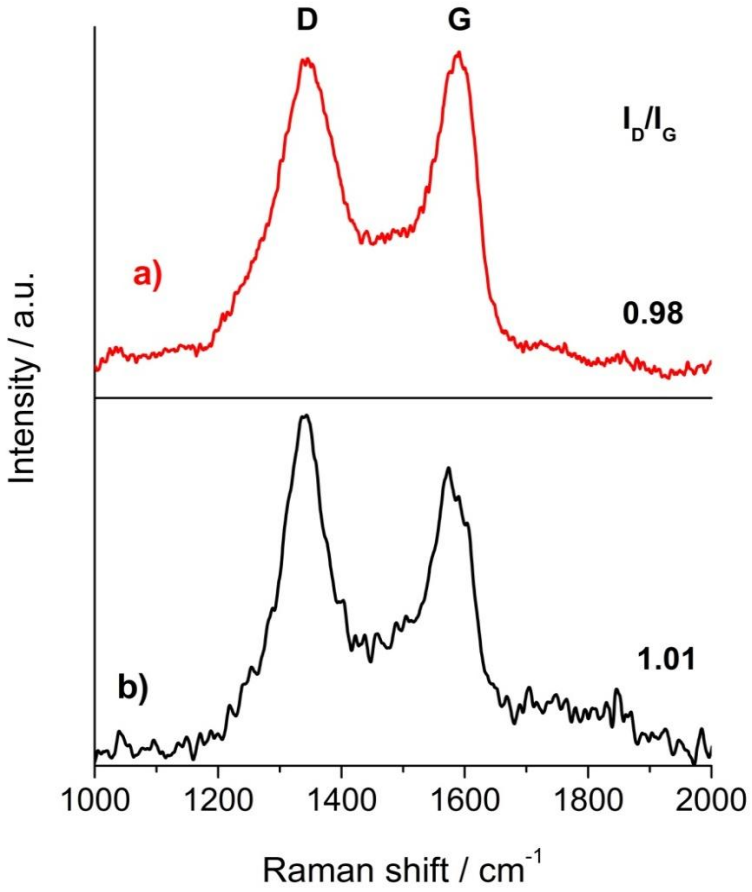

Fig.1. Raman spectra of a) GO and b) RGO obtained after hydrazine-reduction treatment of GO

2.3.2 Morphological, structural and optical properties

The morphological, structural and optical properties characterization were performed to the composite film with the highest photocurrent generated in the phenol oxidation under visible light: the 0.03 wt% boron doped-TiO_2/3 wt% graphene composite film (0.03B-TiO_2/3RGO). TiO_2 and 0.03B-TiO_2 films also were studied for comparative purposes.

Figure 2 shows the typical morphology of the TiO_2, 0.03B-$TiO_2$and 0.03B-TiO_2/3RGO films. 0.03B-TiO_2 and 0.03B-TiO_2/3RGO films exhibit a high number of

cracks than TiO_2 film. The cracked morphology can be associated to the thermal stress in the cooling down stage during the heating process of the films [20]. The average thickness is approximately 288.3 nm, 158.7 nm and 167.6 nm for the TiO_2, 0.03B-TiO_2 and 0.03B-TiO_2/3RGO films. The difference in film thickness can be ascribed to the different amounts of TiO_2 sol retained during the deposition of three film layers before calcination [20, 21].EDS mapping of 0.03B-TiO_2/3RGO composite film (Figure 3) shows that Ti, O, B, and C from the film are homogeneously dispersed. Despite the presence of cracks (dark zones), these are covered with the titanium dioxide film (light zone). In addition Fe, Cr and Ni composition corresponds to 304SS substrate.

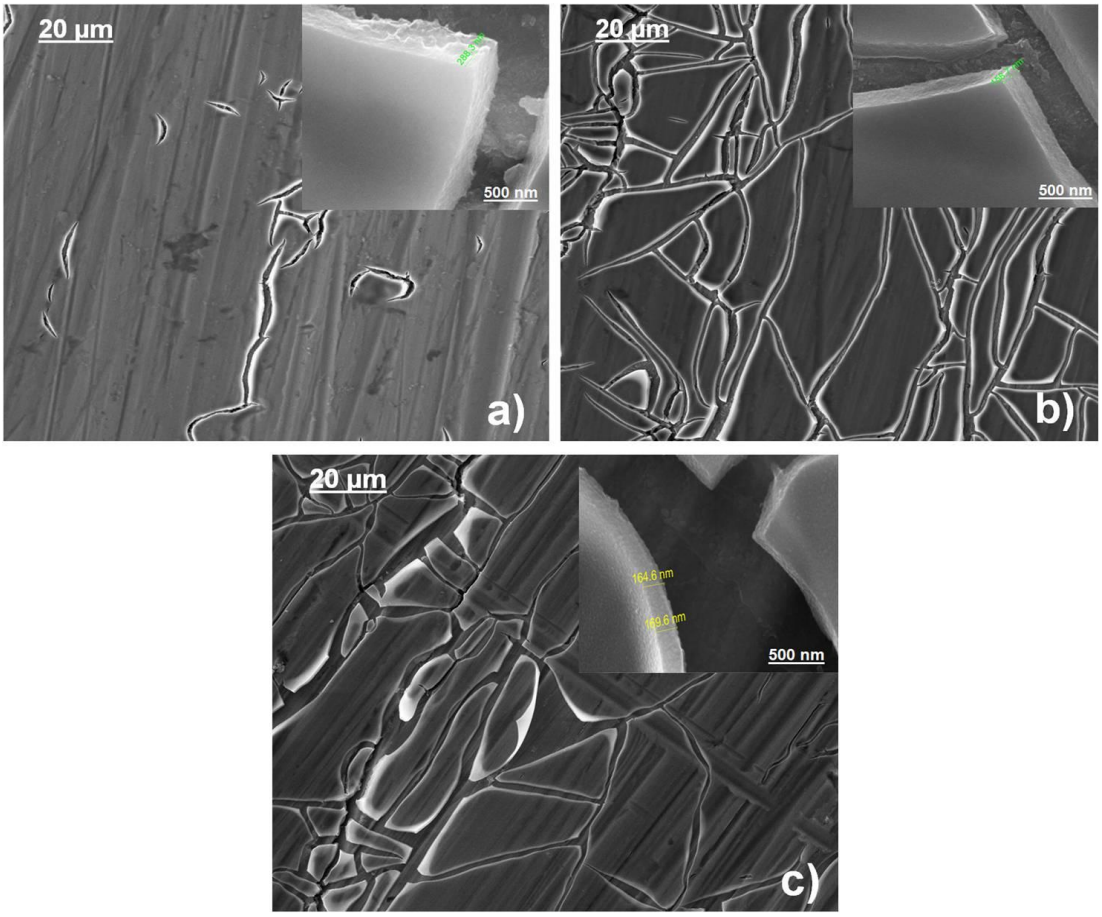

Fig.2. FESEM images of (a) TiO2, (b) 0.03B-TiO2 and (c) 0.03B-TiO2/3RGO films.

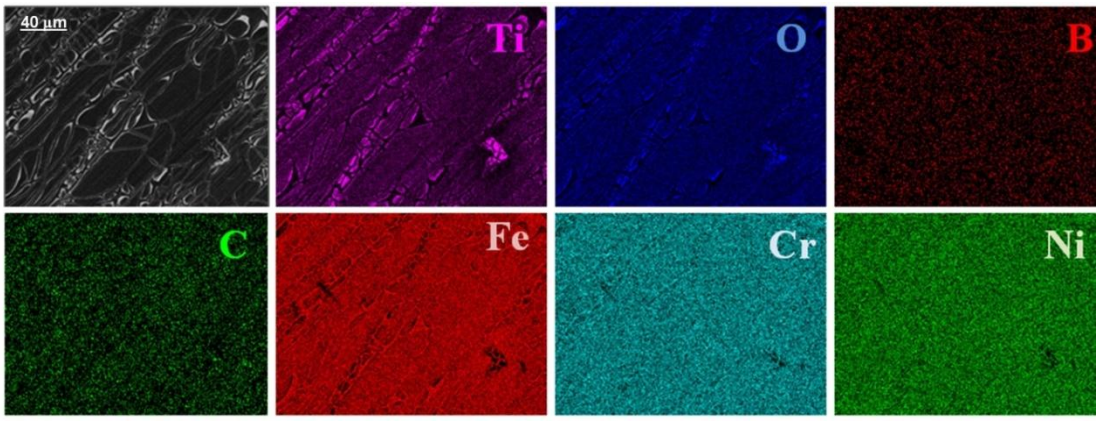

Fig.3. EDS mapping of 0.03B-TiO_2/3RGO composite film.

Figure 4 shows the GIXRD profiles of TiO_2, 0.03B-TiO_2 and 0.03B-TiO_2/3RGO films presents the characteristics reflections (101), (004), (200), (105), (211) and (204) of anatase phase of TiO_2 (PDF-21-1272). Diffraction peaks of doped films are wider and less intense than undoped TiO_2 film. Assuming a spherical shape of particles, the crystallite size (D) is estimated using the Scherrer equation (eq. 1)

$$D = \frac{0.89\lambda}{\beta\cos\theta} \qquad (1)$$

where, λ is the X-ray wavelength of Cu Kα radiation 0.15406 nm, β is the half-value width of (101) anatase peak, and θ is the Bragg angle (in radians) [22, 23]. Average crystalline sizes are 21.25 nm, 17.01 nm and 16.68 nm for TiO_2, 0.03B-TiO_2 and 0.03B-TiO_2/3RGO films, confirming that boron doping inhibits the growth of TiO_2 crystallites. Therefore, these results explain the presence of large cracks in the 0.03B-TiO_2 (Figure 2b) and 0.03B-TiO_2/3RGO (Figure 2c) films compared with the TiO_2 film (Figure 2a). Although the thermal-expansion coefficient (TEC) of the TiO_2 (anatase) is closed to the 304SS to be 11.52 x10^{-6} K^{-1} and 10.2 x10^{-6} K^{-1} respectively, it has been reported that increasing the crystallite size, the TEC also increases [24]. Thus, to decrease the crystallite size of the TiO_2 film after boron doping, its TEC is also decreased. This implies a large difference between the TEC

of the film and the 304SS substrate, which increases the probability of crack formation [21].

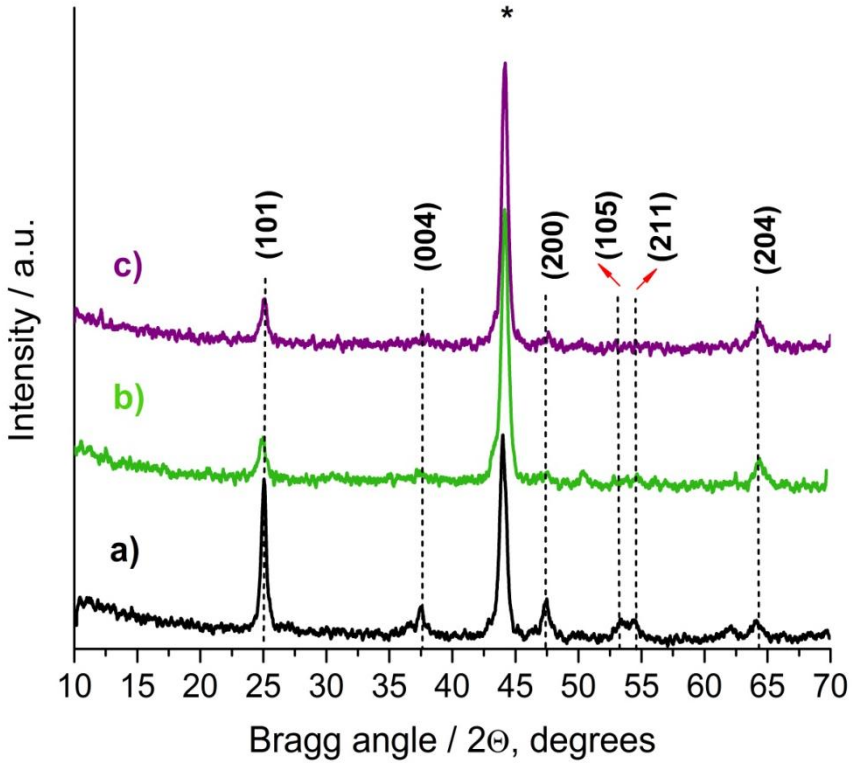

Fig.4. GIXRD patterns of a) TiO2, b) 0.03B-TiO2 and c) 0.03B-TiO2/3RGO. The asterisk corresponds to reflection for 304SS.

Diffraction peaks are not shifted after boron doping, suggesting that boron could occupy interstitial positions within the TiO_2 lattice [22]. Indeed, ionic radius of B^{3+} (0.023 nm) is much smaller than the Ti^{4+} (0.068 nm) [25].

Figure 5 shows the absorption edges of boron-doped films which shift to higher wavelength compared with undoped TiO_2, showing that boron doping enhances the visible light absorption [23]. The shift to higher wavelength values in the 0.03B-TiO_2 films is ascribed to the formation of impurity levels located below of the bottom of the conduction band (CB) of TiO_2 where the electrons are promoted from the valence band (VB) of the semiconductor [7]. Incorporation of RGO in the 0.03B-TiO_2 films modify the optical properties of TiO_2, extending even more the

light absorption to the visible region [26], similar to TiO_2 nanotube hybrid RGO composites and carbon nanotubes doped TiO_2 films, reported in recent works [27]. Modified Kubelka-Munk function is used to estimate the band gap energy of films by plotting $[F(R)hv]^{1/2}$ versus energy of photons (hv) (inset of Figure 5) [23]. Band gap values are 3.28 eV, 2.72 eV and 2.63 eV for TiO_2, 0.03B-TiO_2 and 0.03B-TiO_2/3RGO films respectively. This confirms that boron doping and the incorporation of RGO extent the absorption edge of TiO_2 to the visible light region.

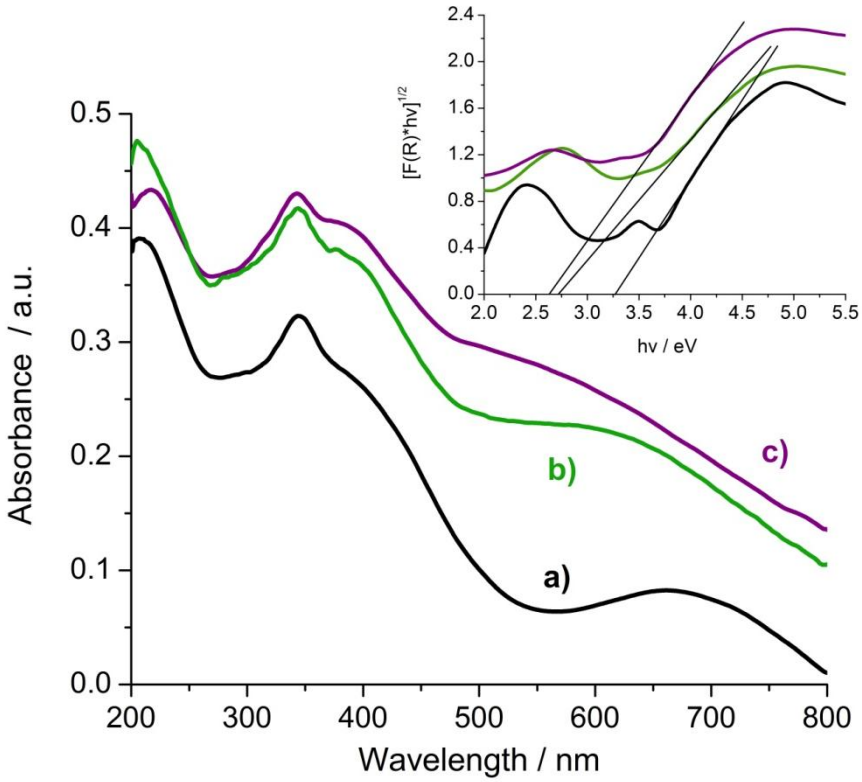

Fig.5. DRS spectra of a) TiO2, b) 0.03B-TiO2 and c) 0.03B-TiO2/3RGO films. Inset: schematic representation of the method for band gap, Eg, determination.

2.3.3 Photoelectrochemical properties

The light absorption capability of TiO_2 is an important feature in the photoelectrochemical (PEC) process due to under illumination, TiO_2 generates charge carriers which can form highly oxidant species in solution and carry out oxidation process [28]. However, the TiO_2 is not active to the visible light which limits its PEC performance. The presence of boron extends the light absorption of TiO_2 films to the visible region according with the characterization of the films discussed above. Thus, the photoelectrochemical measurements can provide information of the enhancement of the light absorption capability of TiO_2 after boron doping.

Figure 6 shows the linear sweep voltammograms started in positive direction from open circuit potential (OCP) in 0.1 M $HClO_4$ and 1 mM phenol + 0.1 M $HClO_4$, for the 0.02B-TiO_2 film. The OCP values from the measurements performed under visible light illumination (Figure 6a, c) are observed to more negative potentials compared with the OCP values obtained from the measurements in the dark (Figure 6b, d). This is due to the electrons in the Fermi level increases their free energy to more negative potentials when the semiconductor exhibits a n-type behavior, indicating that the material is photoactive under visible light [13, 29]. On the other hand, in the anodic polarization curve obtained in presence of phenol under dark conditions (Figure 6b), a faradaic current is observed to potential values closer to 1.25 V, while that in the measurements performed in absence of the organic compound (Figure 6d), the generated current is not significant. Thus, it can be mentioned that the phenol oxidation is recorded in 1.25 V [30, 31]. This implies that a high energy is required to carry out the oxidation process, showing the recalcitrant feature of phenol [30]. However, when the film is illuminated, an initial photocurrent is generated due to the electron/hole pair generation [13]. Therefore, although the generated photocurrent in the photoelectrochemical process (enlargement of Figure 6) exhibits minor magnitude compared with the

electrochemical (EC) process (Figure 8b), the high oxidant power of the photogenerated holes allows the phenol oxidation at a lower potential value (e.g. 0.5 V) compared with the electrochemical process (1.25 V).

In the photoelectrochemical process, the photogenerated holes can react with adsorbed H_2O molecules in the film, forming hydroxyl radicals as follows (eq. 2-4) [28]:

$$B - TiO_2 + H_2O + h^+ \rightarrow B - TiO_2[HO^{\cdot}] + H^+ \quad (2)$$

The organic compound (R) is oxidized (RO) on the film surface:

$$B - TiO_2[HO^{\cdot}] + R \rightarrow B - TiO_2 + RO + H^+ + e^- \quad (3)$$

Or directly react with the holes:

$$B - TiO_2 + h^+ + R \rightarrow B - TiO_2 + RO + e^- \quad (4)$$

Hence, the phenol oxidation can be promoted by indirect (hydroxyl radicals) or direct reaction (holes) requiring a low energy compared with the EC process.

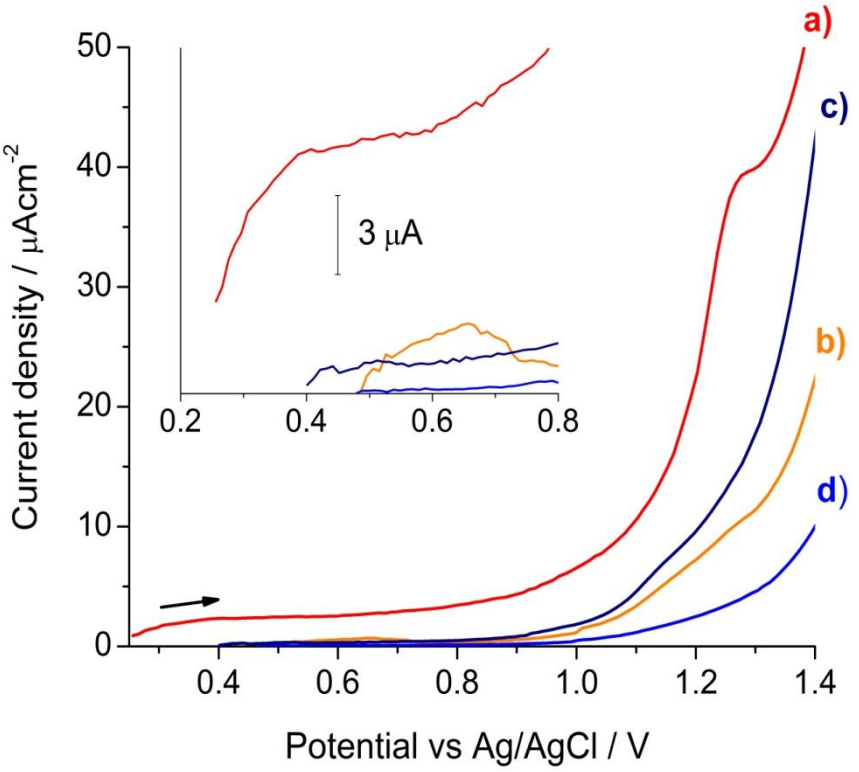

Fig.6. Linear sweep voltammograms (10 mVs-1) obtained in 0.1 M HClO4 in presence and absence of 1 mM phenol for the 0.02B-TiO2 film; a) and c) under visible light illumination, b) and d) in the dark.

Although the charge carrier photogeneration plays an important role in the oxidative capability of TiO_2, the electron transport within the film defines its PEC performance [3-5]. It is well known that TiO_2 exhibit low conducting properties, which can restrain the photogenerated electron transport from the film to the current collector, promoting the charge carrier recombination [9, 26]. In order to increase the conductivity in the B-TiO_2 films and promote the electron transport from the interfase to the back current collector, the incorporation of RGO could avoid the charge carrier recombination, increasing the generated photocurrent. Figure 7 shows the linear sweep voltammograms started in positive direction from open circuit potential (OCP) in presence of 1 mM phenol + 0.1 M $HClO_4$ for the 0.02B-TiO_2/RGO films with different RGO content. When the RGO content is less to 3 wt% (Figure 7a-d), a low initial photocurrent is obtained during the potential

scan from OCP to 0.8 V, but this signal is gradually improved with the increase of the RGO content to 3 wt% (Figure 7e) [3, 4]. This indicates that more photogenerated electrons are transported to the cathode, promoting the charge carrier separation, which increases the generated photocurrent [32, 33]. When the RGO content exceeds 3 wt% the redundant RGO acts as a kind of recombination center, inducing the electron/hole pair recombination in the RGO (Figure 7f, g). Thus, the electron transport is restrained, decreasing the photocurrent again. A similar behavior was observed by Tang et al [32].

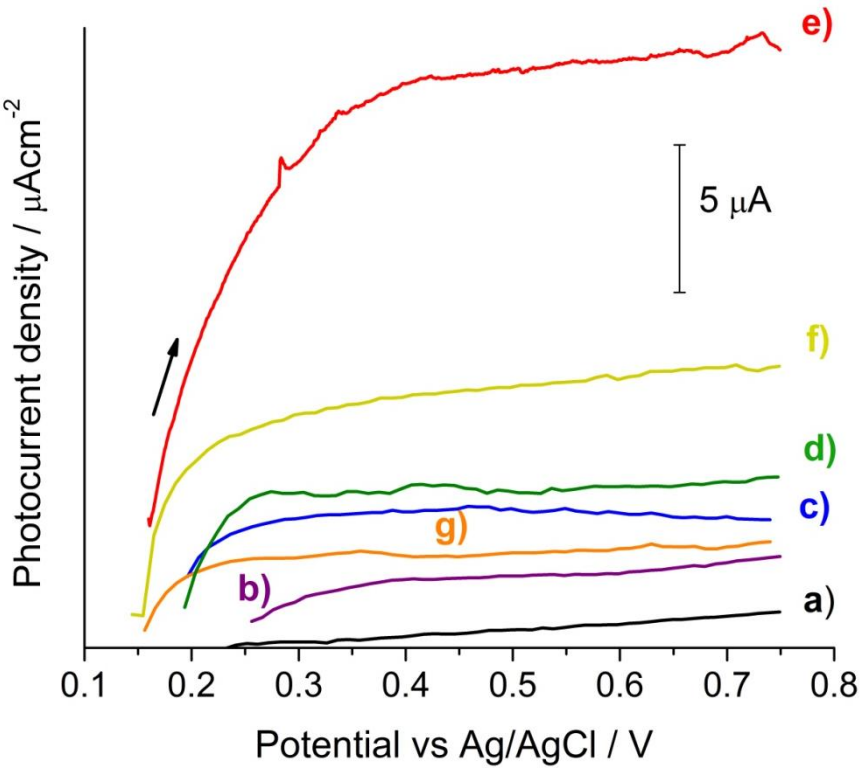

Fig.7. Linear sweep voltammograms (10 mVs^{-1}) obtained in 1 mM phenol and 0.1 M $HClO_4$ under visible light for the a) TiO_2 and b) 0.1B-TiO_2 film and 0.02B-TiO_2/RGO composite films with different RGO content: c) 1 wt%, d) 2 wt%, e) 3 wt%, f) 4 wt% and g) 10 wt%.

As the electron transport is enhanced with the incorporation of an optimal RGO content, the electron/hole pair photogeneration in the semiconductor also can be

improved. Thus, Figure 8 shows the linear sweep voltammograms started in positive direction from open circuit OCP in presence of 1 mM phenol + 0.1 M $HClO_4$ for the B-TiO_2/3RGO composite with different boron content [13]. When the boron content is increase up to 0.03 wt% (Figure 8b), the generated photocurrent is 3 times higher compared with the composite film with 0.02 wt% boron (Figure 8a). Moreover, the photocurrent decreases significantly as the boron content is increased up to 0.04 wt% (Figure 8c). Thus, the 0.03B-TiO_2/3RGO composite film shows the highest generated photocurrent, indicating that more photogenerated electrons are transported to the current collector, leaving more photogenerated holes to promote the formation of hydroxyl radicals or directly react with phenol and carry out the oxidation process [34], although in the case of 0.03B-TiO_2/3RGO and 0.04B-TiO_2/3RGO composite films, a low decrease in the initial photocurrent is exhibited as consequence of the formation of highly resistive Cr_2O_3 at potential value between 0.05 and 0.08 V, hindering the electron transport to the cathode [35]. Even so, the 0.03B-TiO_2/3RGO composite film presents a high conductivity due to the presence of high electron donor states content in the material.

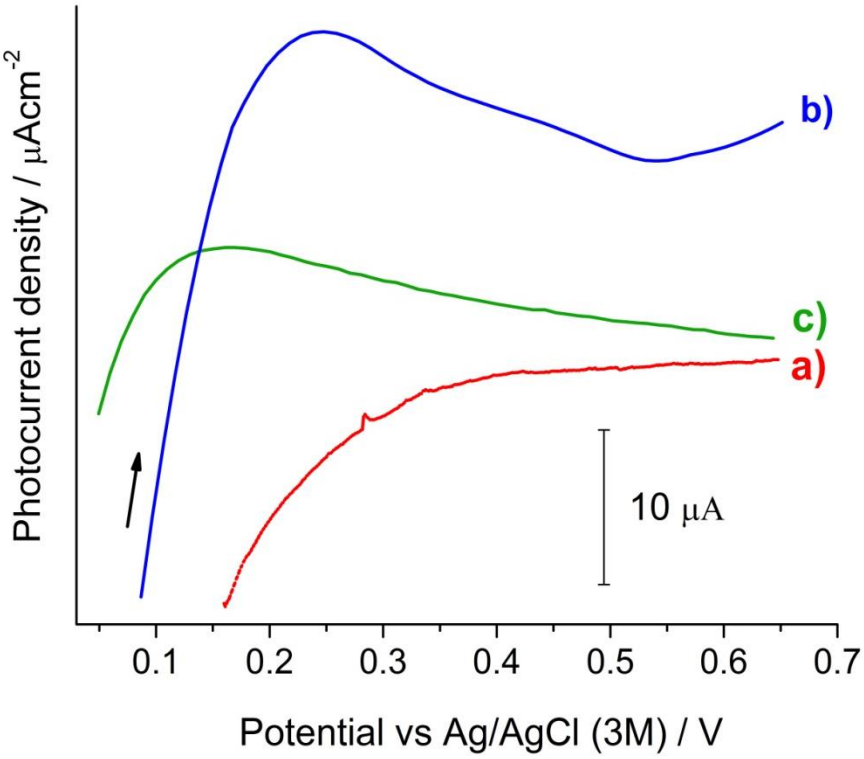

Fig.8. Linear sweep voltammograms (10 mVs^{-1}) obtained in 1 mM phenol and 0.1 M $HClO_4$ under visible light for the B-TiO_2/3RGO composite films with different boron content: a) 0.02 wt%, b) 0.03 wt%, c) 0.04 wt%.

After doping of the TiO_2/3RGO composite film with 0.03 wt% boron, a certain amount of donor states, known as Ti^{3+} species are formed [7]. These states are just below of the bottom of the CB of TiO_2, where the electrons are promoted from the VB of the semiconductor. Therefore, the photoresponse to the visible region is intensified. The Ti^{3+} states transfer the electrons to the CB of TiO_2, diminishing the electron/hole pair recombination, which increases the conductivity in the material [36]. Furthermore, the high holes accumulation in the semiconductor can be promoted, improving the oxidation process under visible light illumination. When the boron content exceeds 0.03 wt%, the remaining Ti^{3+} ion amount acts as strong recombination centers for photogenerated electron/hole pairs, decreasing the generated photocurrent [22]. Hence, the 0.03B-TiO_2/3RGO composite film shows a

superior PEC performance and its photocurrent is 30 times higher compared with the TiO_2 film.

2.3.4 XPS analysis

To evaluate the XPS spectra of the 0.03B-TiO_2/3RGO composite film, it was necessary to employ the following strategy. First, the binding energies (BE) of the B 1s, C 1s and Ti 2p peaks of the film were determined by fixing the Ti-O component of the O 1s peak at 531 eV as reference. This peak was preferred over the adventitious carbon C – C due to the overlapping of this signal and the graphitic carbon besides of oxygen was the predominant element in this type of films.

In order to determinate the composition and chemical state of the 0.03B-TiO_2/3RGO composite film, an XPS analysis was performed (Figure 9). From the general spectrum (Figure 9a) was possible to identify and confirm the presence of Ti, O, C and B (enlargement of Figure 9a) in the composite film, whereas Fe corresponds to 304SS substrate. Figure 9b displays the core-level XPS spectrum of the B 1s. The B 1s appeared at around 192–193 eV. The standard binding energy of B 1s in B_2O_3 or H_3BO_3 equals to 192.0 eV (B-O bond) and in TiB_2 equals to 187.5 eV (B–Ti bond) [23]. The observed XPS spectrum of the B 1s consisted of one peak in 191.9 eV. This suggests that boron was incorporated in the interstitial position of TiO_2 lattice, existing in the form of the B-O-Ti structure [22]. This analysis suggested that the thermal treatment allowed the incorporation of boron atoms into the TiO_2 lattice. The estimated FWHM (in eV) of this peak was 1.66.

Figure 9c, shows the of O 1s photoelectron spectrum that was decomposed in three components. The main one was located in 531.0 eV and was assigned to oxygen bound to titanium (Ti – O) in the TiO_2 lattice (calibration reference) [37], the second component in 532.2 eV was ascribed to oxygen atoms bound to carbon [C – O] and in hydroxyl groups (O – H) [27]. This component was fixed to 1.2 eV to

the Ti – O component. The third component in 533.0 eV was associated to the oxygen doubly bound to carbon in carboxyl [(C=O)-OH] and ester [(C=O)-O-C] functional groups from the RGO [3,27].

On the other hand, The C 1s high-resolution spectrum, Figure 9d, was reconstructed from the decomposition of this in four contributions at 284.1eV, 284.7 eV, 286.2 eV and 288.6 eV. The first peak was attributed to sp^2 carbon (C = C) from the structure of graphene [37]. The second peak was ascribed to adventitious carbon [C – (C, H)] [37, 38], the third peak corresponded to the carbon atoms bounded to oxygen (C – O) [39]. This peak was fixed to 1.5 eV to the second signal. The fourth signal was assigned to the carbon atoms doubly bound to oxygen in carboxyl [(C=O)-OH] and ester [(C=O)-O-C] functional groups [3, 29, 37]. The fraction and the FWHM of the components of the O 1s and C 1s from XPS are showed in Table 2.

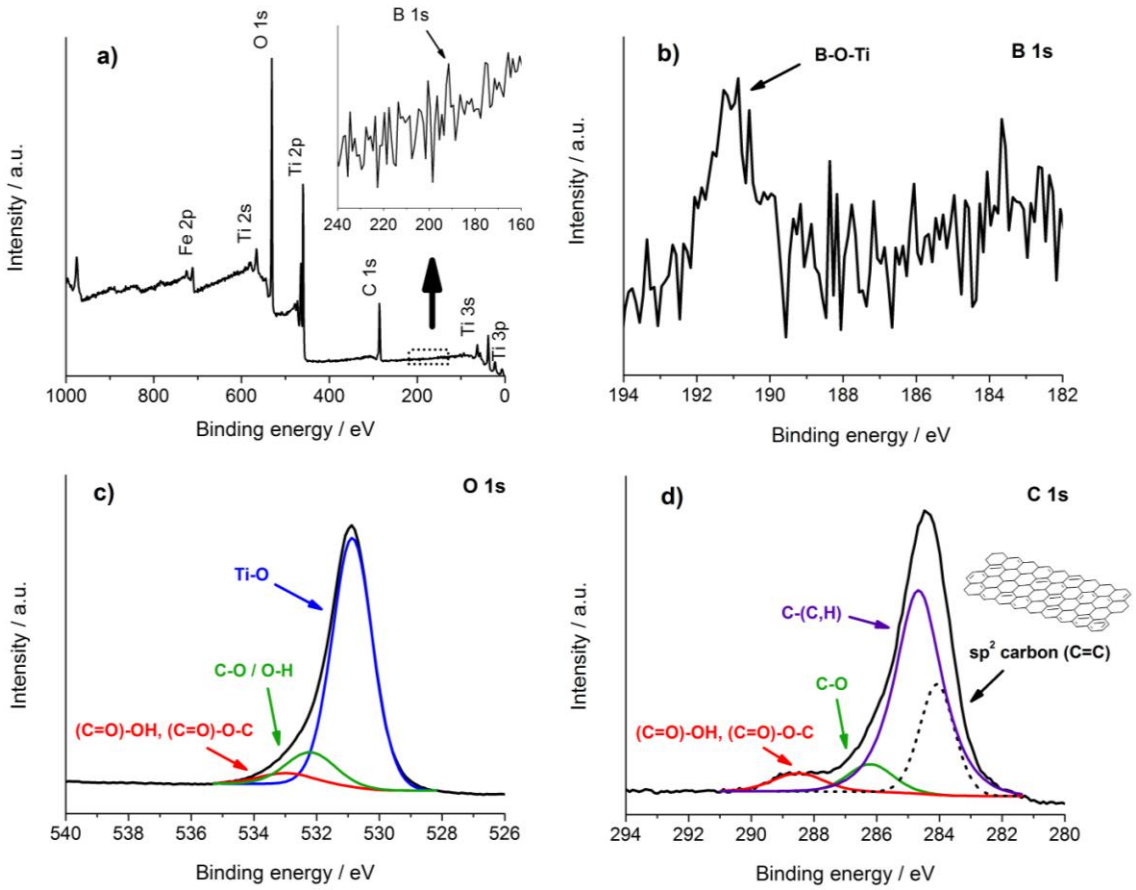

Fig.9. XPS spectra of a) 0.03B-TiO2/3RGO composite film, b) B 1s, decomposition of the c) O 1s and d) C 1s core level.

Table2. Components of the O 1s and C 1s peaks of the 0.03B-TiO2/3RGO composite film from XPS.

O 1s		C1s	
Component	Fraction (FWHM)	**Component**	Fraction (FWHM)
Ti – O (reference calibration)	0.82 (1.57)	**sp^2carbon (C=C)**	0.23 (1.35)
C – O / O – H	0.13 (1.89)	**C – (C, H) (adventitious carbon)**	0.63 (1.80)
(C=O)-OH, (C=O)-O-C	0.05 (2.01)	**C – O**	0.08 (1.80)
		(C=O)-OH, (C=O)-O-C	0.062.01)

Figure 10 shows the decomposition of the Ti 2p core level for the TiO_2, 0.03B-TiO_2 and 0.03B-TiO_2/3RGO films. The Ti 2p doublet spectrum of the 0.03B-TiO_2/3RGO composite film (Figure 10c) exhibited three contributions associated to Ti^{4+}, Ti^{3+} and Ti^{2+}. For Ti^{4+}, the peaks were located at 458.1 eV (Ti $2p_{3/2}$) and 463.8eV (Ti $2p_{1/2}$). For Ti^{3+}, Ti $2p_{3/2}$was located at 456.8 eV and Ti $2p_{1/2}$ at 462.5 eV and for Ti^{2+}, Ti $2p_{3/2}$ and Ti $2p_{1/2}$were located at 456.1 eV and 461.4 eV, respectively [39]. These contributions were also determinated for the TiO_2 (Figure 10a) and 0.03B-TiO_2 films (Figure 10b) for comparative purposes and their atomic concentration are reported in Table 3. The Ti $2p_{3/2}$ and $2p_{1/2}$ for the Ti^{3+} specie were fixed to 1.3 eV to the signals from the Ti^{4+} specie. It can observed that after boron doping both Ti $2p_{3/2}$ and $p_{1/2}$ peaks for each Ti specie not were shifted to higher or lower BE values in the 0.03B-TiO_2 film compared with the TiO_2 film. This indicates that boron could be introduced in interstitial positions within the TiO_2 lattice forming a B-O-Ti type bond, without modify the semiconductor structure [25]. The interstitial boron can donate its valence electrons to Ti^{4+} reducing to Ti^{3+}, increasing the Ti^{3+} species content in the TiO_2 lattice, which was evidenced in the decrease of the Ti^{4+}/Ti^{3+} ratio (Table 4). This is in good accordance with the computational results of Di valentin et al [40], where the presence of interstitial boron in the TiO_2 lattice to induce the formation of Ti^{3+} species was described by DFT calculations. It is well known that Ti^{3+} ions have a dual function, on one hand introducing donor levels below of the bottom of the CB of TiO_2 extending the photoactivity of semiconductor to visible region [7], and acting as photogenerated electron traps decreasing the electron/hole pair recombination [22]. This corroborates the DRS spectra analysis described above.

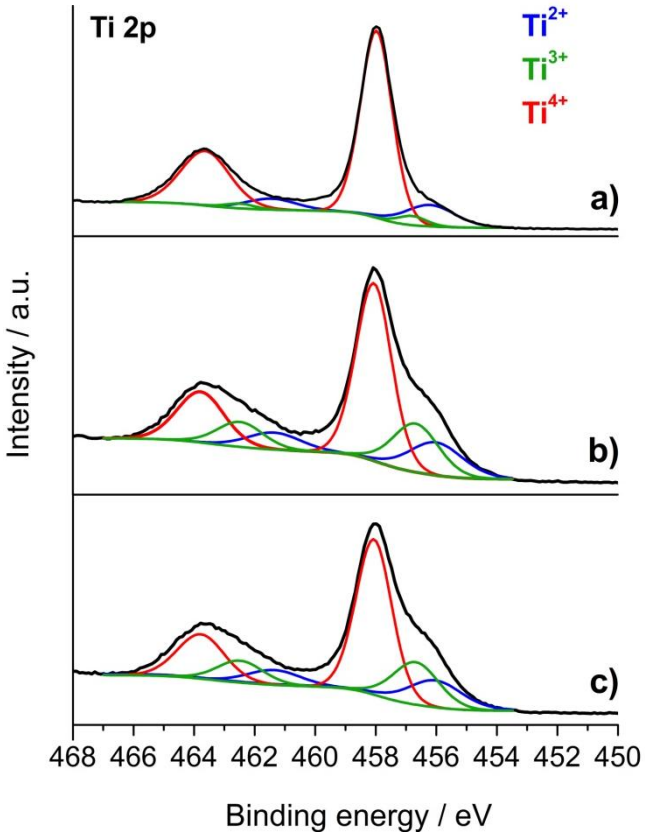

Fig.10. Decomposition of the Ti 2p core level of the (a) TiO2, (b) 0.03B-TiO2 and (c) 0.03B-TiO2/3RGO films.

Table3. Ti 2p representative signals of each Ti chemical species in the films deposited on 304SS.

Films	Ti chemical species signals / eV					
	Ti^{2+} (FWHM)		Ti^{3+} (FWHM)		Ti^{4+} (FWHM)	
	$2p_{3/2}$	$2p_{1/2}$	$2p_{3/2}$	$2p_{1/2}$	$2p_{3/2}$	$2p_{1/2}$
TiO_2	456.0 (2.04)	461.3 (2.04)	456.7 (1.17)	462.4 (1.17)	458.0 (1.28)	463.6 (1.99)
0.03B-TiO_2	456.0 (2.17)	461.3 (2.17)	456.7 (1.85)	462.4 (1.85)	458.0 (1.45)	463.6 (1.90)
0.03B-TiO_2/3RGO*	456.1 (2.13)	461.4 (2.13)	456.8 (1.81)	462.5 (1.81)	458.1 (1.46)	463.7 (1.93)
***increase about 0.1 eV to higher BE**						

Table4. Relative titanium chemical specie fraction and atomic ratios of the films deposited on 304SS from XPS.

Films	Ti chemical species fraction			Atomic ratio		
	Ti^{2+}	Ti^{3+}	Ti^{4+}	B/Ti	C/Ti	O/Ti
TiO_2	0.17	0.03	0.80	-	1.28	2.60
0.03B-TiO_2	0.17	0.21	0.62	0.02	0.75	2.62
0.03B-TiO_2/3RGO	0.17	0.21	0.62	0.02	0.80	2.77

On the other hand, when RGO was incorporated in the films, the $2p_{3/2}$ and $2p_{1/2}$ peaks of each Ti species in the 0.03B-TiO_2/3RGO composite film were shifted towards higher BE values compared with the 0.03B-TiO_2 film. These results strongly indicated that RGO could be coupled with Ti atoms from TiO_2 through the carboxyl and ester groups identified by the XPS spectra of the O 1s and C 1s, forming a Ti-O-C type bond [38]. This affirmation is in good accordance with the report of Chen et al [27], who also proposed the formation of Ti-O-C bond between TiO_2 and RGO in carbon nanotube-doped TiO_2 films by XPS. The TiO_2-RGO couple was the key for the enhancement of electron transport of the 0.03B-TiO_2/3RGO composite film shown above by linear sweep voltammograms.

In order to confirm the presence of interstitial boron and RGO incorporated in the TiO_2 films, the B/Ti, C/Ti, O/Ti ratios were estimated from the atomic composition of each film and exhibited in Table3. The B/Ti ratio implies the presence of boron in the 0.03B-TiO_2 and 0.03B-TiO_2/3RGO films with respect to TiO_2 film. On the other hand, it can observe that the C/Ti ratio for the TiO_2 film was the highest, due to the possible increase of the organic carbon content. In contrast, the decrease in the C/Ti ratio for the 0.03B-TiO_2 and 0.03B-TiO_2/3RGO films suggests a decrease in the organic carbon after boron doping. The slight increase of the C/Ti ratio for the 0.03B-TiO_2/3RGO composite film compared with the 0.03B-TiO_2 film indicates the presence of RGO in the films. The O/Ti ratio in the 0.03B-TiO_2 films remains constant with respect to the TiO_2 film, corroborating that the oxygen atoms in the

TiO_2 lattice were not substituted by boron atoms after doping. However, the O/Ti ratio for the 0.03B-TiO_2/3RGO composite film showed an increase compared with the TiO_2 and 0.03B-TiO_2films due to the possible presence of the oxygen-containing groups from the RGO, increasing the oxygen content in the film.

Hence, a photoactivation mechanism of B-TiO_2/RGO composite film is proposed (Figure 11). Under illumination, the electrons are promoted from the VB of TiO_2 to the Ti^{3+} donor states formed after boron doping, extending the light absorption to visible region. The photoexcited electrons are transfer from these states to the CB and transported to current collector through RGO, leaving more photogenerated holes in the composite film to induce the formation of hydroxyl radicals or react directly with phenol, to promote the oxidation process. Due to RGO is coupled with TiO_2 by Ti-O-C bonds, it serves as efficient acceptor and transporter of photogenerated electrons, improving the electronic transport within the film, inhibits the charge carrier recombination. The formation of Ti^{3+} chemical species by boron doping and the high electrical conduction of RGO generate an increase on the generated photocurrent, which indicates that the photoelectrochemical properties of the B-TiO_2/RGO composite films are enhanced.

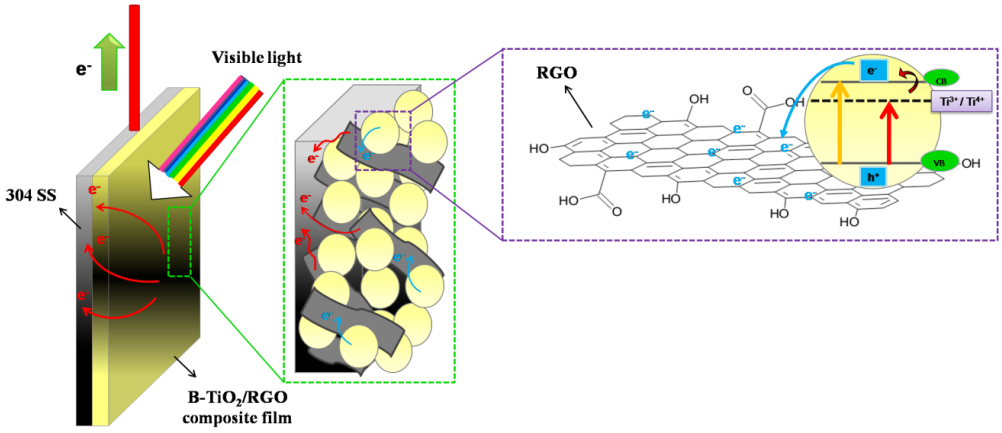

Fig.11. Proposed photoactivation and electron transport mechanism of the B-TiO_2-RGO composite film.

2.4 Conclusions

B-TiO_2/RGO composite films deposited on 304SS were successfully prepared by sol-gel method and dip-coating technique. The high photocurrent generated by the B-TiO_2/RGO composite films is attributed to the improved electron transport within the films. Due to RGO is coupled with TiO_2 by Ti-O-C bonds, RGO acts as an efficient acceptor and transporter of photogenerated electrons, inhibiting the electron/hole pair recombination. Photogenerated electrons are promoted from the VB of TiO_2 to the Ti^{3+} donor states formed by the presence of interstitial boron in the TiO_2 lattice, extending the light absorption to the visible region. These states transfer the electrons to the CB and transported to the current collector, accumulating more holes in the semiconductor to carry out the oxidation process, which inhibits the charge carrier recombination. An excess of boron and RGO content in composite films promotes the formation of recombination centers for photogenerated electron/hole pairs, decreasing the electron transport in the B-TiO_2/RGO composite films. The 0.03B-TiO_2/3RGO composite film exhibits the highest generated photocurrent than 0.03B-TiO_2 and other B-TiO_2/RGO composite films and it is 30 times compared with the TiO_2 film.

References

[1] T. L.Villarreal, Y. Mao, S. S. Wong, R. Gómez, Photoelectrochemicalbehaviour of anatasenanoporous films: effect of the nanoparticle organization. Nanoscale, 2 (2010) 1690–1698.

[2] J. Durantini, P. P. Boix, M. Gervaldo, G. M. Morales, L. Otero, J. Bisquert, E. M. Barea, Photocurrent enhancement in dye-sensitized photovoltaic devices with titania–graphene composite electrodes. J. Electroanal. Chem. 683 (2012) 43–46.

[3] D. Wang, X. Li, J. Chen, X. Tao, Enhanced photoelectrocatalytic activity of reduced graphene oxide/TiO_2 composite films for dye degradation. Chem. Eng. J. 198–199 (2012) 547–554.

[4] P. Wang, Y. Ao, C. Wang, J. Hou, J. Qian, Enhanced photoelectrocatalytic activity for dye degradation by graphene–titania composite film electrodes. J. Hazard. Mater. 223–224 (2012) 79–83.

[5] J.M. Macak, H. Tsuchiya, A. Ghicov, K. Yasuda, R. Hahn, S. Bauer, P. Schmuki, TiO_2 nanotubes: Self-organized electrochemical formation, properties and applications Curr. Opin. Solid State Mater. Sci. 11 (2007) 3–18.

[6]Y. Hua, W. Jing, Z. ShanQing, L. XinJun, Z. HuiJun, Layered Fe(III) doped TiO2thin-film electrodes for the photoelectrocatalytic oxidation of glucose and potassium hydrogen phthalate. Chinese Sci. Bull. August 56 (2011) 2475–2480.

[7]L. Liu, Y. Li, Understanding the Reaction Mechanism of Photocatalytic Reduction of CO_2 with H_2O on TiO_2-Based Photocatalysts: A Review. *Aerosol* air Qual. Res.14 (2014) 453–469.

[8] W. Shu, Y Liu, Z. Peng, K. Chen, C. Zhang, W. Synthesis and photovoltaic performance of reduced graphene oxide-TiO_2 nanoparticles composites by solvothermal method. Chen, J. Alloy Compd. 563 (2013) 229-233.

[9] C. Liu, Y. Teng, R. Liu, S. Luo, Y. Tan, L. Chen, Q. Cai, Fabrication of graphene films on TiO_2 nanotube arraysforphotocatalytic application. Carbon. 49 (2011) 5312–5320.

[10] G. Liu, X. Wang, L. Wang, Z. Chen, F. Li, G. Qing (Max) Lu, H. M. Cheng, Drastically enhanced photocatalytic activity in nitrogen doped mesoporous TiO_2 with abundant surface states. J. Colloid Interf. Sci. 334 (2009) 171–175.

[11] Y. Lv, L. Yu, X. Zhang, J. Yao, R. Zou, Z. Dai, P-doped TiO_2 nanoparticles film coated on ground glass substrate and the repeated photodegradation of dye under solar light irradiation. Appl. Surf. Sci. 257 (2011) 5715–5719.

[12] A. Zaleska, E. Grabowska, J. W. Sobczak, M. Gazda, J. Hupka, Photocatalytic activity of boron-modified TiO_2 under visible light: The effect of boron content, calcination temperature and TiO_2 matrix Appl. Catal., B. 89 (2009) 469–475.

[13] Lu, H. Zhao, J. Li, X. Quan, S. Chen, Characterization of boron-doped TiO_2 nanotube arrays prepared by electrochemical method and its visible light activity. Sep. Purif. Technol. 62 (2008) 668–673.

[14] W.S. Hummers, R.E. Offeman, Preparation of Graphitic Oxide.J. Am. Chem. Soc. 80 (1958) 1339.

[15] R.D. Martínez-Orozco, H.C. Rosua, Soo-Wohn Lee, V. Rodríguez-González, Understanding the adsorptive and photoactivity properties of Ag-graphene oxide nanocomposites. J. Hazard. Mater. 263 (2013) 52–60.

[16] D. Li, M. B. Muller, S. Gilje, R. B. Kanerand, G. G. Wallace, Processable aqueous dispersions ofgraphenenanosheets. Nat. Biotechnol. 3 (2008) 101 – 105.

[17] S. Li, Q. Wang, T. Chen, Z. Zhou, Y. Wang, J. Fu,Study on cerium-doped nano-TiO_2 coatings forcorrosion protection of 316 L stainless steel, Nanoscale Res. Lett. 7 (2012) 1–9.

[18]K. Krishnamoorthy, M. Veerapandian, G. Kimand, S. J. Kim, A One Step Hydrothermal Approach for the Improved Synthesis of GrapheneNanosheets. Curr. Nanosci. 8 (2012) 934-938.

[19]Z. Bo, X. Shuai, S. Mao, H. Yang, J. Qian, J. Chen, J. Yan, K. Cen, Green preparation of reduced graphene oxide for sensing and energy storage applications, Sci. Rep. 4 (2014) 4684.

[20] N. Barati, M.A. FaghihiSani, H. Ghasemi, Z. Sadeghian, S.M.M. Mirhoseini, Preparation of uniform TiO_2 nanostructure film on 316L stainless steel by sol–gel dip coatingAppl. Surf. Sci. 255 (2009) 8328–8333.

[21] L. Lopez, W. A. Daouda, D. Duttaa, B. C. Panther, T. W. Turney, Effect of substrate on surface morphology and photocatalysis of large-scale TiO_2 films. Appl. Surf. Sci. 265 (2013) 162-168.

[22] X. Lu, B. Tian, F. Chen, J. Zhang, Preparation of boron-doped TiO_2 films by autoclaved-sol method at low temperature and study on their photocatalytic activity. Thin Solid Films 519 (2010) 111–116.

[23] J. Ding, Y. Yuan, J. Xu, J. Deng, J. Guo, TiO_2Nanopowder Co-Doped with Iodine and Boron toEnhance Visible-Light Photocatalytic Activity, J. Biomed.Nanotechnol. 5 (2009) 1–7.

[24] N. Jagtap, M. Bhagwat, P. Awati, V. Ramaswamy, Characterization of nanocrystallineanatasetitania: an in situ HTXRD study. Thermochim. Acta 427 (2005) 37–41.

[25] Chen, D. Yang, Q. Wang, Z. Jiang, Effects of Boron Doping on Photocatalytic Activity and Microstructure of Titanium Dioxide Nanoparticles. Ind. Eng. Chem. 45 (2006) 4110–4116.

[26] G. Li, T. Wang, Y. Zhu, S. Zhang, C. Mao, J. Wu, B. Jin, Y. Tian, Preparation and photoelectrochemical performance of Ag/graphene/TiO_2 composite film. Appl. Surf. Sci. 257 (2011) 6568–6572.

[27] C. Chen, Y. C. Ho, W.S. Guo, C.M. Huang, T.C. Pan, Enhanced visible light-induced photoelectrocatalytic degradation of phenol by carbon nanotube-doped TiO_2 electrodes. Electrochem. Acta 54 (2009) 3884–3891.

[28] R. T. Pelegrini,R. S. Freire, N. Duran, R. Bertazzoli, Photoassisted Electrochemical Degradation of Organic Pollutants on a DSA Type Oxide

Electrode: Process Test for a Phenol Synthetic Solution and Its Application for the E1 Bleach Kraft Mill Effluent. Environ. Sci. Technol. 35 (2011) 2849-2853.

[29] X. Dong, J. Tao, Y. Li, H. Zhou, Enhanced Photoelectrochemical Properties of F-containing TiO2 sphere thin film induced by its novel hierarchical structure. Appl. Surf. Sci. 255 (2009), 7183–7187.

[30] L. Bao, R. Xiong, G. Wei, Electrochemical polymerization of phenol on 304 stainless steel anodes and subsequent coating structure analysis. Electrochim. Acta 55 (2010) 4030–4038.

[31]J. Iniesta, P.A. Michaud, M. Panizza, G. Cerisola, A. Aldaz, Ch. Comninellis, Electrochemical oxidation of phenol at boron-doped diamond electrode. Electrochim. Acta 46 (2001) 3573 – 3578.

[32] Y.B. Tang, C.S. Lee, J. X. Zeng-Tao Liu, Z. H. Chen, Z. He, Y. L. Cao, G. Yuan, H. Song, L. Chen, L. Luo, H. L. Cheng, W. J. Zhang, I. Bello, S. T. Lee, Incorporation of Graphenes in Nanostructured TiO_2 Films via Molecular Grafting for Dye-Sensitized Solar Cell Application. ACS Nano 4 (2010) 3482–3488.

[33] N. Yang, J. Zhai, D. Wang, Y. Chen, L. Jiang, Two-Dimensional Graphene Bridges Enhanced Photoinduced Charge Transport in Dye-Sensitized Solar Cells. ACS Nano 4 (2010) 887–894.

[34] N. Lu, X. Quan, J. Y. Li, S. Chen, H. T. Yu, G.H. Chen,Fabrication of Boron-Doped TiO_2 Nanotube Array Electrode and Investigation of Its Photoelectrochemical Capability J. Phys. Chem. 111 (2007) 11836–11842.

[35]G. Goodlet, S. Faty, S. Cardoso, P.P. Freitas,A.M.P. Simoes, M.G.S. Ferreira, M. Da Cunha Belo, The electronic properties of sputtered chromium and iron oxide films. Corros. Sci. 46 (2004) 1479–1499.

[36] G. Yang, Z. Jiang, H. Shi, T. Xiao, Z. Yan, Preparation of highly visible-light active N-doped TiO_2photocatalyst. J. Mater. Chem., 20 (2010) 5301–5309.

[37] N.R. Khalid, Z. Honga, E. Ahmed, Y. Zhang, H. Chan, M. Ahmad, Synergistic effects of Fe and graphene on photocatalytic activity enhancement of TiO_2 under visible light. Appl. Surf. Sci. 258 (2012) 5827–5834.

[38] N.R. Khalid, E. Ahmed, Z. Hong, M. Ahmad, Synthesis and photocatalytic properties of visible light responsive La/TiO_2-graphene composites. Appl. Surf. Sci. 263 (2012) 254–259.

[39] P. Acevedo-Peña, L. Lartundo-Rojas, I. González,Effect of water and fluoride content on morphologyand barrier layer properties of TiO_2 nanotubes grown in ethylene glycol-based electrolytes J. Solid. State Electrochem. 17 (2013) 2939–2947.

[40] C. Di Valentin, G. Pacchioni, Trends in non-metal doping of anatase TiO_2: B, C, N and F. Catal. Today 206 (2013) 12–18.

CHAPTER 3: EFFECT OF SUBSTRATE ON THE PHOTOELECTROCHEMICAL ACTIVITY OF BORON-DOPED TIO_2/GRAPHENE COMPOSITE FILMS IN THE PHENOL OXIDATION UNDER UV-VIS LIGHT ILLUMINATION

Abstract

In this chapter, the effect of the substrate on the photoelectrochemical activity of the 0.03 wt% boron-doped TiO_2/3wt% graphene composite films deposited on 304 stainless steel (304SS) and titanium (Ti) plates in the phenol oxidation under UV-vis light illumination is studied. The films were prepared by sol-gel method and dip-coating technique. The surface of the composite films was characterized by FESEM, GIXRD and XPS. OCP measurements indicate that the composite films exhibit a n-type semiconductor behavior under illumination. However, the composite film deposited on Ti presents a major generated photopotential than the film deposited on 304SS due to low electron trapping, facilitating the electronic transport and the photogenerated charge carrier separation. The high electron trapping in the composite film on 304SS is attributed to the presence of acceptor states detected by Mott-Schottky plots, which promote the electron/hole pair recombination, decreasing the photoelectrochemical activity of the film. This can be evidenced in a low photocurrent observed by linear sweep voltammetry measurements. Cyclic voltammetry and photocurrent transient measurements display that composite film deposited on Ti shows to be more photoelectrochemically active in a prolonged time than the composite film deposited on 304SS. The photoelectrochemical phenol oxidation using the composite film on Ti is about twice more effective than the film deposited on 304SS.

3.1 Introduction

Titanium dioxide (TiO_2) is a powerful n-type semiconductor employed in the environmental purification today. Its photoactivity comes from the high oxidant power of the holes generated when this material is illuminated [1], promoting the formation of radical species in solution to carry out the pollutant oxidation [2, 3]. Thus, TiO_2 has been widely studied in suspension form for photocatalytic clean-up of contaminated wastewaters [3, 4]. However, the separation of TiO_2 particles from the treated water poses several problems including loss of photoactive material and fouling by suspended solids, which accumulate with the recycled TiO_2 particles, decreasing its photoactivity by reuse [4]. The preparation of TiO_2 films deposited on conducting substrates is an alternative to overcome these disadvantages and extend its industrial applications such as the photoelectrochemical (PEC) oxidation of pollutants in wastewaters [5] or dye-sensitized solar cells [6]. In PCE processes, when the TiO_2 film employed as photoanode is illuminated, the electron/hole (e^-/h^+) pairs are generated, promoting the holes accumulation in the semiconductor while the electrons are transported within the film to the conducting substrate or current collector where the film is deposited, generating a photocurrent [7]. However, the TiO_2 exhibit important problems such as: (1) it is only active to the UV irradiation, limiting its PCE performance [3], (2) presents low conducting properties, hindering the electron transport which promotes the charge carrier recombination [5] and (3) the TiO_2 based films are obtained from suspensions which can exhibit low adherence occasioning the detachment of the film from the current collector [8]. In the previous chapter, boron-doped TiO_2/graphene composite films (B-TiO_2/RGO) were prepared by the sol-gel method with the aim of the dip-coating technique on 304SS with the purpose of enhance the PEC performance of TiO_2 for the phenol oxidation under visible light illumination. The presence of boron extended the light absorption to the visible region, increasing its electron/hole pair photogeneration capability of TiO_2 while the RGO incorporation improved the electron transport within the film,

promoting the charge carrier separation, which was evidenced in an increase of the generated photocurrent. The composite films were obtained from B-TiO_2/RGO sol solutions to enhance the homogeneity and the adherence of the film on the current collector.

Although, the PEC properties of the TiO_2 films can be enhanced, an important aspect to study is the conducting substrate. The nature of substrate has been shown to be essential in the preparation of the TiO_2 films [9]. Ambat et al [10] reported the study of the photoelectrochemical properties of TiO_2 films deposited on 316L stainless steel (S316L) and aluminum alloy (AA1050) by DC magnetron sputtering, indicating that the TiO_2 on S316L exhibit higher photoelectrochemical activity than the film deposited in AA1050, due to the multiple donor states within of band gap of TiO_2 by the presence of Fe_2O_3 in TiO_2-substrate interfase, but the photogenerated charge carrier separation is hindered by the presence of Cr_2O_3, under UV light exposure. Thus, the choice of the type of conducting substrate can be a determinant factor on the PEC activity of TiO_2.

In this chapter, the effect of substrate on the PEC activity of the boron-doped TiO_2/graphene (B-TiO_2/RGO) composite films for the phenol oxidation is studied. This effect was investigated by voltammetry, photocurrent transients and OCP measurements under UV-Vis light illumination. Mott-Schottky measurements were performed in absence of phenol to investigate the semiconducting properties of the composite films. Films were deposited on 304SS and Ti plates by sol-gel method and dip-coating technique, being 0.03 wt% boron doped TiO_2/3 wt% RGO (0.03B-TiO_2/3RGO) the best preparation of B-TiO_2/RGO sol to obtain composite films with high PEC properties under visible light illumination, reported in the previous chapter. The morphology and the crystalline phase of the 0.03B-TiO_2/3RGO composite films deposited on both substrates are also presented.

3.2 Experimental

3.2.1 Preparation of the 0.03B-TiO_2/3RGO composite films

The 0.03B-TiO_2/3RGO sol solution was prepared by sol-gel process with a procedure reported in the previous chapter. 304 SS and Ti plates were ground with No. 120, 240, 320 and 600 emery papers, and cleaned by sonication with ethanol and acetone. The 0.03B-TiO_2/3RGO composite films were deposited by the dip-coating technique in both substrates at a rate of 60 mm/min, followed by dehydration at 100°C. The deposition and thermal treatment was repeated 3 times in order to prepare films with high adherence [11]. Finally, the films were calcined at 400°C with a constant heating rate of 3°C/min and kept for 90 min. The geometric area was 0.765 cm^2.

3.2.2 Characterization of 0.03B-TiO_2/3RGO composite films

The surface morphology of the 0.03B-TiO_2/3RGO composite films deposited on both 304SS and Ti substrates, 0.03B-TiO_2/3RGO/304SS and 0.03B-TiO_2/3RGO/Ti, respectively was analyzed by field scanning electron microscopy (FESEM) using a JOEL Quanta 650 FEG equipped equipped with an EDAX Apollo X energy dispersive X-ray spectroscopy (EDS). The grazing incidence X-ray diffraction (GIXRD) profiles of the films were recorded using a Bruker D8 Discover diffractometer with Da Vinci geometry operated at 40 kV and 30 mA, using Cu Kα radiation (0.15406 nm) selected with Ni filter, in grazing incidence mode with a step of 0.015° and a counting time of 1.0 s per step. The analysis of the phases present in the composite film was analyzed by comparing the observed profile with the patterns reported in the PDF-2 database of the International Centre for Diffraction Data (ICDD). X-ray photoelectron spectroscopy (XPS) spectra were carried out through Thermo Scientific K-alpha X-ray photoelectron spectrometer

with an Al Kα X-ray source (1.487 eV). Carbon C 1speak is usually a good way to detect and compensate the charge shift effect. Unfortunately, carbon is not the main component of the film surfaces. Since oxygen is the predominant element in this type of films, O 1s peak is more suitable to detect and compensate the charge shift. Hence, the binding energy of XPS spectra was calibrated with reference to the O 1s peak (531 eV). Gaussian-Lorentzian mix function and Shirley background subtraction were employed to deconvolute the XPS Ti 2p, O 1s and C 1s spectra. Collected XPS spectra correspond to an average of three measurements in different points of each simple.

3.2.3 Photoelectrochemical properties of the 0.03B-TiO_2/3RGO composite films

Photoelectrochemical properties of the 0.03B-TiO_2/3RGO/304SS and 0.03B-TiO_2/3RGO/Ti composite films were investigated in a three-electrode photoelectrochemical cell with a BAS Epsilon potentiostat. A graphite bar was used as counter electrode and a saturated calomel electrode (SCE) as reference electrode. The electrolyte used was 0.1 M $HClO_4$ dissolved in deionized water as a supporting electrolyte at pH 1. Dissolved oxygen was removed from all solutions by bubbling nitrogen. The volume filled in the cell was 40 mL. The UV-Vis light source was a 100 W Xe lamp (Orion instruments), kept at a distance of 30 cm from the films. Open circuit potential (OCP) measurements were measured by irradiating the sample in solution intermittently with UV-Vis light, and the resulting potential was measured using the SCE electrode. Linear sweep voltammetry (LSV) curves were recorded at a scan rate of $10mVs^{-1}$ and each measurement was done in duplicate. Cyclic voltammetry (CV) measurements were performed at a scan rate of $10mVs^{-1}$ during 10 cycles from OCP in both anodic and cathodic direction. Photocurrent measurements were carried out with an anodic potential of 0.85 V vs SCE during 10 min and four ON/OFF light cycles. All the electrochemical

experiments were performed in presence and absence of 1 mM phenol at room temperature.

3.2.4 Mott-Schottky measurements

The determinations of charge carriers density and flat-band potentials of the 0.03B-TiO_2/3RGO/304SS and 0.03B-TiO_2/3RGO/Ti composite films were derivated from analysis of Mott-Schottky plots, which were obtained by performing a potential scan in the cathodic direction. The capacitance measurements were carried out at 100 mV of signal amplitude, at a constant frequency of 7 KHz. The potential range was -0.1 to 0.9 V vs SCE, where the generated photocurrent is capacitive. The measurements were carried out using an E&GG 283 potentiostat (Princeton Applied Research, PAR 283) coupled to a Solartron frequency analyzer model SI 1260. Each measurement was done in duplicate. The experiments were performed in presence of 0.1 M $HClO_4$ and the dark.

3.2.5 Photoelectrochemical phenol oxidation

The photoelectrochemical process was carried out in a three-electrode cell containing the 0.03B-TiO_2/RGO/304SS and the 0.03B-TiO_2/RGO/Ti composite films with an exposed surface area of 0.765 cm^2 as working electrodes. A graphite rod and SCE electrode were used as counter and reference electrodes, respectively. The phenol oxidation was preformed with the same UV-Vis light source described before. A stirred 1 mM phenol solution with 0.1 M $HClO_4$ was used as the solution (total volume of 40 mL). The photoelectrochemical experiments were conducted under anodic potential of 0.85 Vvs SCE, using a BAS Epsilon potentiostat. The phenol oxidation was monitored with an Ocean optics USB4000 spectrophotometer using a peristaltic pump. The absorbance of the phenol was evaluated at a wavelength of 270 nm each 30 min. Subsequently, the geometry area was increased to 3.0 $cm^2$and illuminated with visible light with the

purpose of observe the PEC activity of the composite films under this irradiation. In this case, a two-electrode cell was employed to carry out the oxidation process. The visible light source was a 150 W metal halide lamp (MHN-TD Philips) with UV-block. A stainless steel sheet was used as counter electrode. A stirred 1 mM phenol solution with 0.1 M $HClO_4$ was used as the solution (total volume of 40 mL). The photoelectrochemical experiments were conducted under anodic potential of 0.85 V, using an Agilent 08001Apower supply. The absorbance of the phenol was also evaluated at a wavelength of 270 nm each 30 min. The phenol oxidation was monitored using a Shimadzu PC 2401 UV-Vis spectrophotometer.

3.3 Results and discussion

3.3.1 FESEM images

Figure 1 shows the typical morphology for the 0.03B-TiO_2/3RGO composite film deposited on both 304SS and Ti substrates. It can observe that the 0.03B-TiO_2/3RGO/304SS composite film (Figure1a) displays a highly cracked surface compared with the 0.03B-TiO_2/3RGO/Ti composite film (Figure 1b). The cracked morphology is attributed to the shrinkage during the thermal treatment due to the differences between the thermal-expansion coefficients (TEC) of the film and each substrate [11, 12]. The TEC of the TiO_2film is closed to the TEC of the 304SS to be $11.59x10^{-6}$ K^{-1} and $10.2x10^{-6}$ K^{-1}, respectively [9]. This indicates that the composite film deposited on 304SS has less possibility of crack formation. However, a high difference between the TEC of TiO_2 film and the Ti is observed due to the TEC of the Ti is reported to be $5.0x10^{-6}$ K^{-1} [13]. This difference implies a high possibility to form large cracks or fractures during the thermal stress. The average thickness is approximately 158.0 nm and 346.2 nm for the 0.03B-TiO_2/3RGO/304 and 0.03B-TiO_2/3RGO/Ti films. Figure 1c, d display the surface of the 0.03B-TiO_2/3RGO/304 and 0.03B-TiO_2/3RGO/Ti composite films, respectively after the PEC phenol oxidation under an anodic bias potential of 0.85 V. it can be noted that the films not

present adsorbed products on its surface, indicating that under this potential, the PEC oxidation process is carried out trough of the reaction between phenol and the high oxidant photogenerated holes or the physisorbed hydroxyl radicals on the composite film surface, avoiding the fouling or passivation effect which can present to higher potential values [14, 15]. The average thickness is approximately 215.4 nm and 306.6 nm for the 0.03B-TiO_2/3RGO/304 and 0.03B-TiO_2/3RGO/Ti composite films, respectively. The difference in film thickness can be ascribed to the different amounts of TiO_2 sol retained during the deposition of the films before calcination [9].

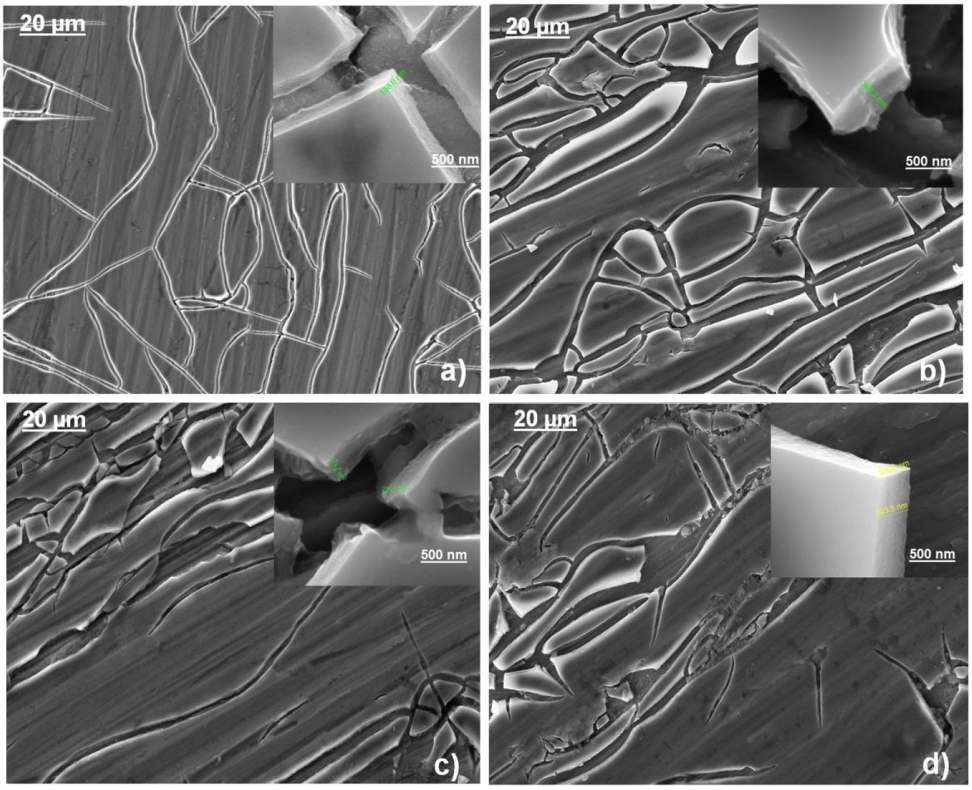

Fig.1. FESEM images of the 0.03B-TiO_2/3RGO/304SS and 0.03B-TiO_2/3RGO/Ti composite films a) and b) before, c) and d) after the PEC phenol oxidation.

3.3.2 GIXRD analysis

The GIXRD profile of the 0.03B-TiO_2/3RGO/Ti composite film is shown in Figure 2. Compared with the GIXRD profile of Ti substrate, the 0.03B-TiO_2/3RGO/Ti composite film displays a signal at a Bragg angle of 25.22° for the reflection (101) peak attributed to the anatase form of TiO_2 in the composite film. The GIXRD profile for the 0.03B-TiO_2/3RGO/304SS composite film exhibited in the previous chapter shows the same reflection (101) peak at a Bragg angle of 25.13°. This indicates that the nature of the substrate no induce changes in the crystalline phase of TiO_2. Assuming a spherical shape of the particles, the crystallite size (D) is estimated using the Scherrer equation (eq. 2)

$$D = \frac{0.89\lambda}{\beta\cos\theta} \qquad (2)$$

where, λ is the X-ray wavelength of Cu Kα radiation (0.15402 nm), β is the half-value width of (101) anatase peak, and θ is the Bragg angle (in radians) [16, 17]. The average crystallite size for the 0.03B-TiO_2/3RGO/Ti composite film is 10.74 nm. The crystallite size of the 0.03B-TiO_2/3RGO/Ti composite film is lower than the 0.03B-TiO_2/3RGO/304SS composite film (16.68 nm), due to the Ti substrate at high temperatures also can form a TiO_2 layer, which could facilitate the oxygen diffusion between the composite film and the Ti substrate, which can increase the oxygen vacancies into the TiO_2 lattice of the film [18]. On the other hand, the 0.03B-TiO_2/3RGO/304SS and the 0.03B-TiO_2/3RGO/Ti composite films are doped with the same boron content (0.03 wt%) suggesting that the Ti^{3+} specie content in the TiO_2 lattice of the 0.03B-TiO_2/3RGO/Ti film can be increased due to the formation of these vacancies during the thermal treatment.

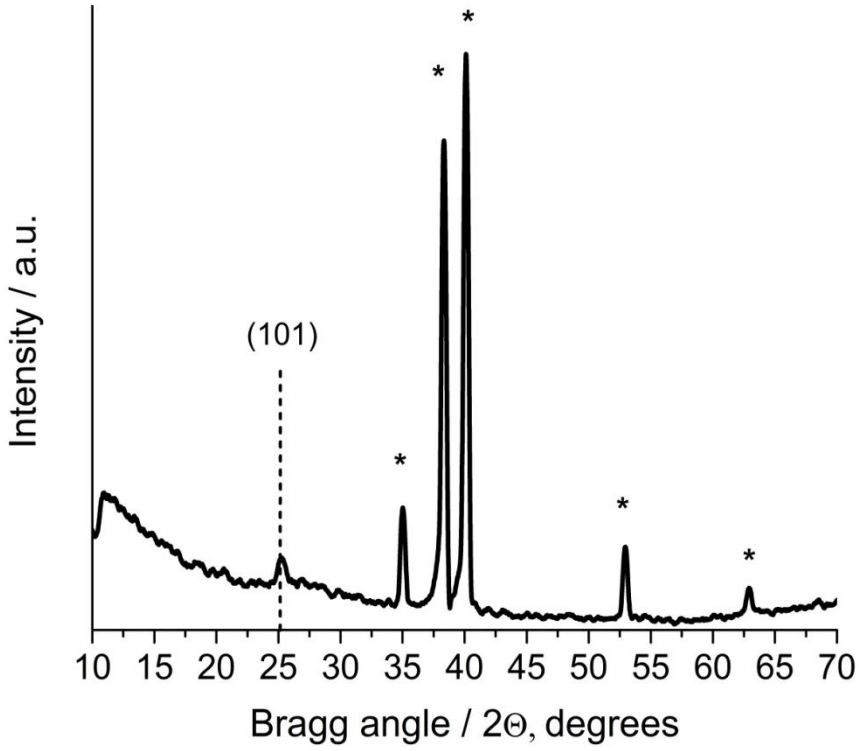

Fig.2. GIXRD patterns of 0.03B-TiO_2/3RGO/Ti composite film. The asterisk corresponds to reflection for Ti.

3.3.3 XPS analysis

To evaluate the XPS spectra of the 0.03B-TiO_2/3RGO/Ti composite film, it was necessary to employ the following strategy. First, the binding energies (BE) of the B 1s, C 1s and Ti 2p peaks of the film were determined by fixing the Ti-O component of the O 1s peak at 531 eV as reference. This peak was preferred over the adventitious carbon C – C due to the overlapping of this signal and the sp^2 carbon besides of oxygen was the predominant element in this type of films.

In order to determinate the composition and chemical state of 0.03B-TiO_2/3RGO/Ti composite film (Figure 3), XPS analysis was performed. From the general spectrum (Figure 3a) was possible to identify and confirm the presence of Ti, O, C

and B (enlargement of Figure 3a) in the composite film. The Figure 3b displays the core-level XPS spectrum of B 1s, which is composed by three contributions: 188.8 eV, 190.5 eV and 191.2 eV. The standard binding energies of B 1s reported in the literature are: 193.6 eV in B_2O_3 (B-O bonds), 193.0 eV in H_3BO_3 and 188.2 eV in TiB_2 (Ti-B bonds) [16]. The first peak was associated to B-Ti bonds in the TiB_2 [17] and the second peak was attributed to O-Ti-B bonds [16,19]. These signals imply the incorporation of boron in sustitucional positions in the TiO_2 lattice, occupying the oxygen vacancies formed during the thermal treatment. The third peak corresponded to the formation of B-O-Ti bonds, indicating that boron was also incorporated in interstitial positions of the TiO_2 lattice [16].

Figure 3c, shows the of O 1s photoelectron spectrum that was decomposed in three components. The main one was located in 530.0 eV and was assigned to oxygen bound to titanium (Ti – O) in the TiO_2 lattice (calibration reference) [20,21], the second component in 532.0 eV was ascribed to oxygen atoms bound to carbon [C – O] and in hydroxyl groups (O – H) [21]. This component was fixed to 1.2 eV to the Ti – O component. The third component in 532.9 eV was associated to the oxygen doubly bound to carbon in carboxyl [(C=O)-OH] and ester [(C=O)-O-C] functional groups from the RGO [21,22].

On the other hand, The C 1s high-resolution spectrum, Figure 3d, was reconstructed from the decomposition of this in four contributions at 284.1eV, 284.6 eV, 286.4 eV and 288.5 eV. The first peak was attributed to sp^2 carbon (C = C) from the structure of graphene [20]. The second peak was ascribed to adventitious carbon [C – (C, H)] [21], the third peak corresponded to the carbon atoms bounded to oxygen (C – O) [22]. This peak was fixed to 1.5 eV to the second signal. The fourth signal was assigned to the carbon atoms doubly bound to oxygen in carboxyl [(C=O)-OH] and ester [(C=O)-O-C] functional groups [21-23]. The fraction and the FWHM of the components of the B 1s, O 1s and C 1s from XPS are showed in Table 1.

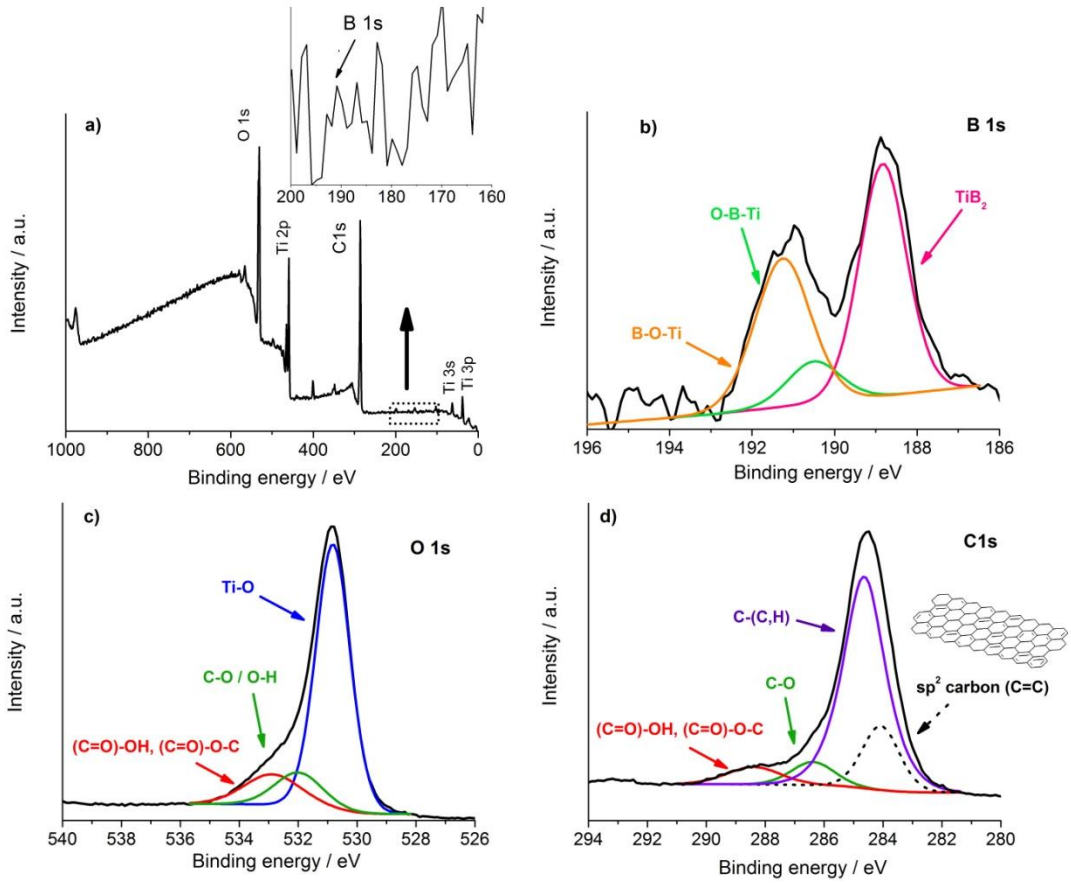

Fig.3. XPS spectra of a) 0.03B-TiO2/3RGO/Ti composite film, b) B 1s, decomposition of the c) O 1s and d) C 1s core level.

Table1. Components of the O 1s and C 1s peaks of the 0.03B-TiO_2/3RGO composite film from XPS.

B 1s		O 1s		C1s	
Component	Fraction (FWHM)	**Component**	Fraction (FWHM)	**Component**	Fraction (FWHM)
TiB_2	0.51 (1.40)	**Ti – O (reference calibration)**	0.73 (1.43)	**sp^2 carbon (C=C)**	0.17 (1.35)
O-Ti-B (substitutional boron)	0.09 (1.57)	**C – O / O – H**	0.14 (1.98)	**C – (C, H) (adventitious carbon)**	0.69 (1.80)
B-O-Ti (interstitial boron)	0.40 (1.66)	**(C=O)-OH, (C=O)-O-C**	0.13 (2.35)	**C – O**	0.07 (1.80)
				(C=O)-OH, (C=O)-O-C	0.07 (2.01)

Figure 4 shows the decomposition of the Ti 2p core level for the TiO_2, 0.03B-TiO_2 and 0.03B-TiO_2/3RGO films deposited on Ti. The Ti 2p doublet spectrum of the 0.03B-TiO_2/3RGO composite film (Figure 4c) exhibited three contributions associated to Ti^{4+}, Ti^{3+} and Ti^{2+}. For Ti^{4+}, the peaks are located at 458.1 eV (Ti $2p_{3/2}$) and 463.8 eV (Ti $2p_{1/2}$). For Ti^{3+}, Ti $2p_{3/2}$ is located at 456.8 eV and Ti $2p_{1/2}$ at 462.5 eV and for Ti^{2+}, Ti $2p_{3/2}$ and Ti $2p_{1/2}$ peaks are located at 455.6 eV and 461.3 eV respectively [24,25]. These contributions were also determinated for the TiO_2 (Figure 4a) and 0.03B-TiO_2 films (Figure 4b) for comparative purposes and their atomic concentration are reported in Table 2. The Ti $2p_{3/2}$ and $2p_{1/2}$ for the Ti^{3+} specie were fixed to 1.3 eV to the signals from the Ti^{4+} specie. It can observed that after boron doping both Ti $2p_{3/2}$ and $p_{1/2}$ peaks for each Ti specie not were shifted to higher or lower BE values in the 0.03B-TiO_2 film compared with the TiO_2 film. This indicates that boron could be introduced in interstitial positions within the TiO_2 lattice forming a B-O-Ti type bond, without modify the semiconductor structure [16,17]. The interstitial boron can donate its valence electrons to Ti^{3+} reducing to Ti^{2+}, increasing the Ti^{2+} species content in the TiO_2 lattice, which was evidenced in the decrease of the Ti^{3+}/Ti^{2+} ratio (Table 3). Although Ti^{2+} is also a donor state, the Ti^{3+} states are present in high proportion and the content is approximately the same for each analyzed film. Furthermore, after boron doping, the Ti^{4+} content is not considerably modified, which indicates that the Ti^{3+} species are formed during the thermal treatment, by the increase of the oxygen vacancies where boron can be also substitutionally incorporated to form O-Ti-B and Ti-B bonds in the TiO_2 lattice [16,19]. Ti^{3+} ions are well known by introducing donor levels below of the bottom of conduction band extending the photoactivity of semiconductor to visible region and act as photogenerated electron traps decreasing the electron/hole pair recombination [27]. Thus, due to the Ti^{3+} content for the 0.03B-TiO_2/3RGO/Ti composite (Table 3) is higher than 0.03B-TiO_2/3RGO/304SS composite film, (Table 4 of the chapter II) the 0.03B-TiO_2/3RGO/Ti composite film could exhibit better PEC properties in the phenol oxidation than the 0.03B-TiO_2/3RGO/304SS composite film.

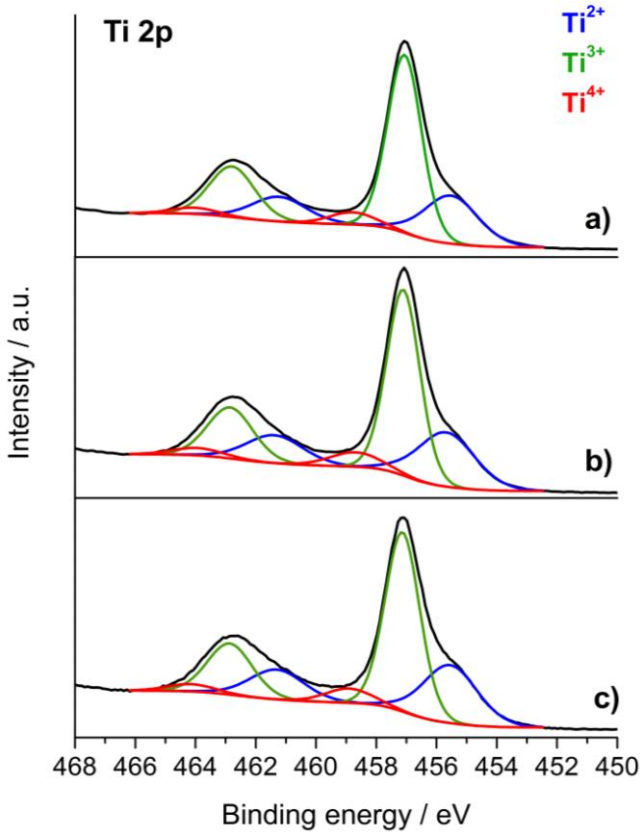

Fig.4. Decomposition of the Ti 2p core level of the (a) TiO2, (b) 0.03B-TiO2 and (c) 0.03B-TiO2/3RGO films deposited on Ti.

Table2. Ti 2p representative signals of each Ti chemical species in the films deposited on Ti.

Films	Ti chemical species signals / eV					
	Ti^{2+} (FWHM)		Ti^{3+} (FWHM)		Ti^{4+} (FWHM)	
	$2p_{3/2}$	$2p_{1/2}$	$2p_{3/2}$	$2p_{1/2}$	$2p_{3/2}$	$2p_{1/2}$
TiO_2	455.5 (2.20)	461.2 (2.20)	456.7 (1.38)	462.4 (1.84)	458.0 (1.84)	463.7 (1.84)
0.03B-TiO_2	455.5 (2.30)	461.2 (2.30)	456.7 (1.35)	462.4 (1.85)	458.0 (2.05)	463.7 (2.05)
0.03B-TiO_2/3RGO*	455.6 (2.20)	461.3 (2.20)	456.8 (1.42)	462.5 (1.82)	458.1 (1.89)	463.8 (1.89)
***increase about 0.1 eV to higher BE**						

Table3. Relative titanium chemical specie fraction and atomic ratios of the films deposited on Ti from XPS.

Films	Ti chemical species fraction		
	Ti^{2+}	Ti^{3+}	Ti^{4+}
TiO_2	0.28	0.66	0.06
0.03B-TiO_2	0.31	0.62	0.07
0.03B-TiO_2/3RGO	0.31	0.62	0.07

On the other hand, when RGO was incorporated in the films, the $2p_{3/2}$ and $2p_{1/2}$ peaks of each Ti species in the 0.03B-TiO_2/3RGO composite film were shifted towards higher BE values compared with the 0.03B-TiO_2 film. These results strongly indicated that RGO could be coupled with Ti atoms from TiO_2 through the carboxyl and ester groups identified by the XPS spectra of the O 1s and C 1s, forming a Ti-O-C type bond. This affirmation is in good accordance with the report of Chen et al [20], who also proposed the formation of Ti-O-C bond between TiO_2 and RGO in carbon nanotube-doped TiO_2 films by XPS.

3.3.4 Photoelectrochemical properties of the 0.03B-TiO_2/3RGO composite films

The best electrochemical method for investigating the photocatalytic properties is monitoring the variation in open circuit potential (OCP) with and without UV-Vis light. The potential shift (Fermi level shift) when the films are exposed to UV-Vis light represents the charge development in the system, when electrons and holes are formed, independent of the surface area. Thus, Figure 5 shows the influence of the UV-Vis light on the open circuit potential (OCP) of the 0.03B-TiO_2/3RGO/304SS and 0.03B-TiO_2/3RGO/Ti composite films in presence and absence of phenol. When a TiO_2 film is illuminated, the electron/hole pairs are generated. The electrons are promoted to the conduction band (CB) of the semiconductor, generating a decrease in the OCP values [27] while the holes

accumulated in the valence band (VB) of TiO_2 travel to the semiconductor-electrolyte solution interfase to react with adsorbed water molecules to highly oxidant species as hydroxyl radicals. These radicals can oxidize adsorbed species on the semiconductor surface. On the other hand, the holes also can oxidize the adsorbed species directly [27, 28]. Meanwhile, the electrons in the CB can reduce the oxygen to form superoxide anion radicals [28]. Thus, the 0.03B-TiO_2/3RGO composite films deposited on 304SS and Ti substrates exhibit an n-type semiconductor behavior.

In absence of phenol, the shift in the OCP value to more negative potentials is due to the photoexcitation of electrons from the VB to the Ti^{3+} donor states located below of the bottom of CB of TiO_2, indicating that the materials are photoactive under UV-Vis light. This shift is denominated photopotential (ΔV_{oc}). Subsequently, these donor states promote electrons to the CB [27]. According with the XPS results of Ti 2p, the Ti^{3+} species content in the 0.03B-TiO_2/3RGO/Ti composite film (Table 3) is higher than the 0.03B-TiO_2/3RGO/304SS (Table 4 of the chapter II) which indicates that an increase of the electron accumulation in the 0.03B-TiO_2/3RGO/Ti composite film (Figure 5a) generating a higher photopotential compared with the 0.03B-TiO_2/3RGO/304SS composite film when the light is ON. Besides of the low Ti^{3+} donor states content in the 0.03B-TiO_2/3RGO/304SS composite film (Figure 5b), the presence of electron traps or recombination centers can hinder the electron accumulation, generating a low photopotential [29]. On the other hand, when the light is OFF, the OCP rapidly relaxes back to the initial value for the 0.03B-TiO_2/3RGO/Ti composite film, confirms a low electron trapping, allowing the return of electrons to the VB of TiO_2 [27].

In presence of phenol, the potential transients before the illumination for the composite films are shifted to more positive potentials, indicating that the charge transfer between the composite films to the solution can occur to reach the electrochemical equilibrium [27]. This shift can suggest that the depletion layer is presented in the composite films. When the light is ON, the 0.03B-TiO_2/3RGO/Ti

composite film (Figure 5c) exhibits the same behavior, but the generated photopotential is higher compared with the photopotential obtained in absence of phenol [30] (Table 4). This indicates that holes accumulated in the VB collect electrons from the phenol when this is oxidized, promoting more electrons to the Ti^{3+} donor states and subsequently to CB [28]. Therefore, the electron accumulation in the semiconductor is increased. This effect can be also observed in the 0.03B-TiO_2/3RGO/304SS composite film (Figure 5d), but the OCP is not relaxed back to the initial value when the light is OFF, confirming the presence of electron traps or recombination centers, restraining the return of the electrons to the VB of TiO_2 [29, 31]. Hence, the photocatalytic properties of film deposited on Ti is superior compared with the film on 304SS.

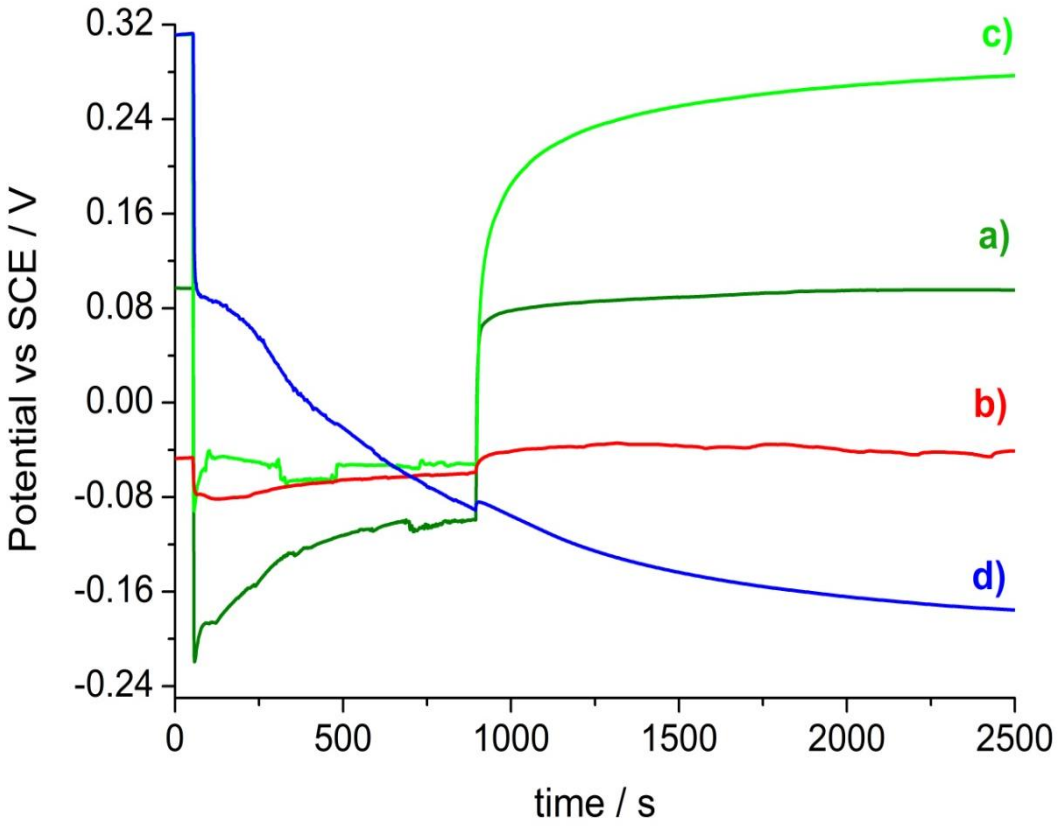

Fig.5. OCP measurements for the 0.03B-TiO2/3RGO/304SS and 0.03B-TiO2/3RGO/Ti composite films a) and b) in absence of phenol; c) and d) in presence of phenol.

Table4. Photopotential generated by the composite films in absence and presence of phenol

Composite film	ΔV_{oc} absence of phenol / V	ΔV_{oc} presence of phenol / V
0.03B-TiO_2/3RGO/304SS	0.03	0.40
0.03B-TiO_2/3RGO/Ti	0.21	0.37

Although the photocatalytic properties of the composite films can be enhanced depending on the nature of the conducting substrate, the electron transport in the TiO_2 film-interfase defines the PEC performance of the film in the oxidation process. Hence the electrochemical measurements under illumination are an important tool to study in the effect of the conducting substrate or as well known as current collector on the PEC behavior of the films.

Figure 6 shows the linear sweep voltammograms of the 0.03B-TiO_2/3RGO/304SS and 0.03B-TiO_2/3RGO/Ti composite films started in anodic direction from OCP in 1 mM phenol + 0.1 M $HClO_4$. The OCP values from the measurements performed under visible light illumination (Figure 6a, c) are observed to more negative potentials compared with the OCP values obtained from the measurements in the dark (Figure 6b, d), confirming the n-type behavior and the photoactivation of the films under this irradiation [32]. When the potential is scanned between OCP and 1.0 V, an initial photocurrent is generated in both composite films under visible light, compared with the low current in the dark. This means that in this potential range in the dark, the composite films are not photoelectrochemically active and the photocurrent observed under illumination is obtained by the electron/hole pair generation [3]. However, the 0.03B-TiO_2/3RGO/Ti composite film (Figure 6a) generates 3.2 times more photocurrent than the 0.03B-TiO_2/3RGO/304SS composite film (Figure 6c). Due to the high chromium content in the 304SS (13-18%), a highly resistive Cr_2O_3 passive layer is formed during the thermal treatment,

inhibiting the photogenerated electron transport in the films, which hinder the charge carrier separation [29].

In contrast, the high photocurrent generated by 0.03B-TiO_2/3RGO/Ti is caused for the facilitated electron transport within the film, promoting the electron/hole pair separation [34, 35]. The Ti substrate collects the photogenerated electrons which are transported to the cathode, leaving more holes accumulated in the film to carry out the oxidation process with high effectiveness. These results suggest that the 0.03B-TiO_2/3RGO/Ti composite film can be more photoelectrochemically active in a prolonged time than the 0.03B-TiO_2/3RGO/304SS composite film.

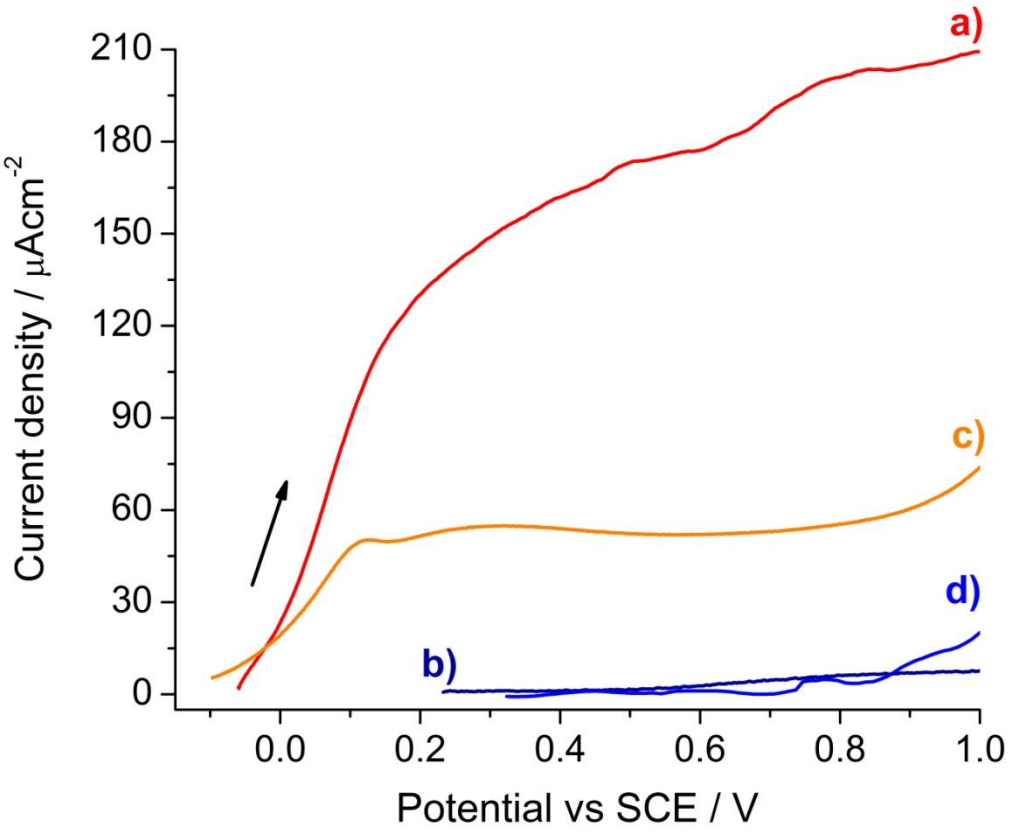

Fig.6.Linear sweep voltammograms (10 mVs-1) obtained in 0.1 M HClO4 in presence and absence of 1 mM phenol for the 0.03B-TiO2/3RGO/Ti and 0.03B- TiO2/3RGO/304SScomposite film; a) and c) under visible light illumination, b) and d) in the dark, respectively.

In order to observe the PEC properties of the composite films in a prolonged time, Figure 7 exhibits the cyclic voltammograms were obtained in anodic direction from OCP to 1.5 V in 1 mM phenol + 0.1 M $HClO_4$ during 10 cycles. The 0.03B-TiO_2/3RGO/304SS composite film (Figure 7a) presents a low photocurrent generated due the resistive feature of the 304SS, hindering the electron transport and the charge carrier separation. Thus, the photocurrent decreases after each cycle [15].When the potential is scanned at potentials over 1.0 V, an increase in photocurrent can be observed, due to the phenol oxidation is carried out in a photoassisted electrochemical process depending only on the applied potential [14].In contrast, for the 0.03B-TiO_2/3RGO/Ti composite film(Figure 7b),the photocurrent not exhibit a significant decrease after each cycle, indicating that the phenol oxidation is carried out in a photoelectrocatalytic process through the holes accumulated in the semiconductor or hydroxyl radicals produced by water oxidation with the holes [33]. Thus, it can be clearly observed that the film deposited on Ti present better PEC properties in the oxidation process than the composite on the 304SS in prolonged time [36].

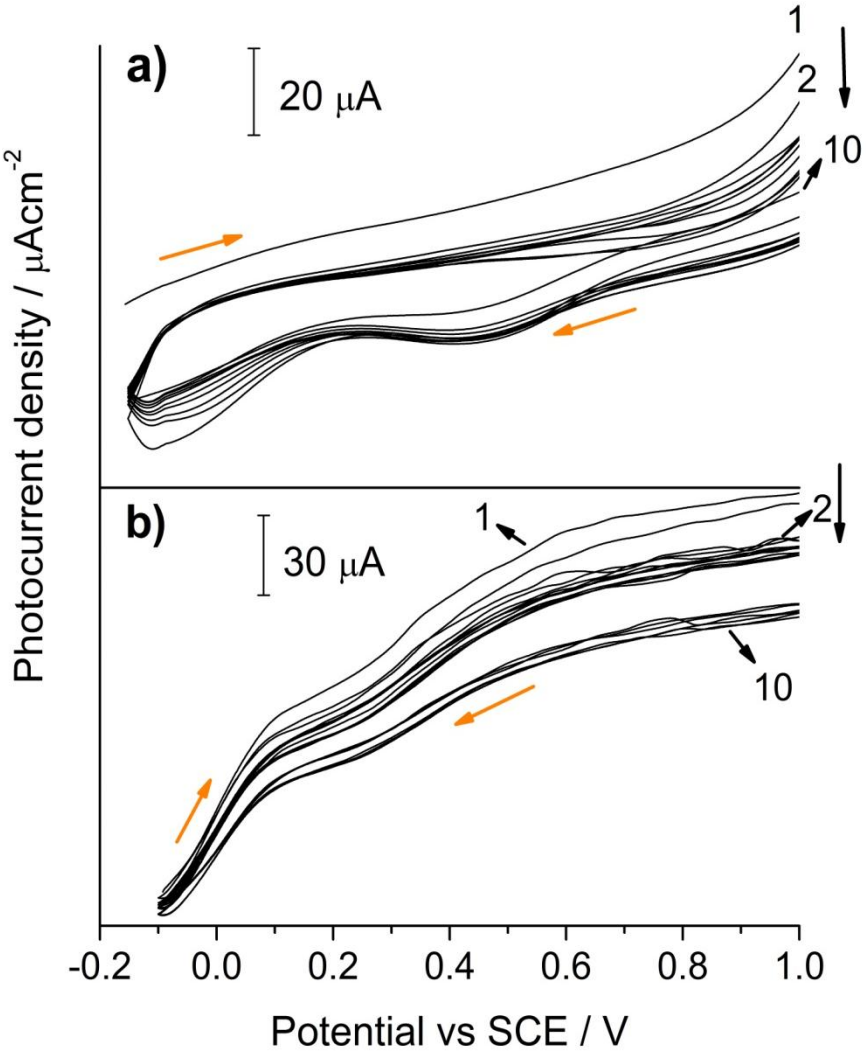

Fig.7. Cyclic voltammograms(10 mVs^{-1}, 10 cycles) obtained in anodic direction in 0.1 M $HClO_4$in presence of 1 mM phenol for the a) 0.03B-TiO_2/3RGO/Ti and b) 0.03B-TiO_2/3RGO/304SS composite film under the UV-Vis light.

On the other hand, Figure 8 displays the cyclic voltammograms of the composite films obtained by potential scan in cathodic direction in 0.1 M $HClO_4$ under the dark. At more negative potentials than -0.4 V, the composite films exhibit a capacitive behavior, typical of nanocrystalline TiO_2 [34]. This behavior is associated to the electron accumulation in the CB of TiO_2 or the filling of surface

states below of CB. For the 0.2B-TiO_2/3RGO/Ti composite film (Figure 8a), the generated current is not decreased after 10 cycles, indicating the absence of any resistance of faradaic process [31]. Furthermore, this composite film exhibit a voltammetric signal at ~ 0 V (enlargement of Figure 8a) associated to states localized within the band gap of the composite film [31, 34]. After the second cycle, this signal disappears. These states can be attributed to the Ti^{3+} donor species formed in the TiO_2 lattice, which facilitates the electron accumulation in the 0.03B-TiO_2/3RGO/Ti composite film [37]. For the 0.03B-TiO_2/3RGO/304SS composite film (Figure 8b), the capacitive current diminishes as consequence of the oxidation of iron and chromium species from the 304SS substrate (enlargement of Figure 8b). After each cycle, the anodic peaks at -0.05 V and 0.12 V associated to the oxidation of iron and chromium species are increased, but a cathodic peak is not increased during the measurements, indicating that the oxidation of Fe and Cr is an irreversible process. On the other hand, a representative signal is observed at about ~0.07 V. This signal is also associated to Ti^{3+} but this peak is not diminished, which means that the electron accumulation or the filling of these states is hindered [38].This can be consequence of recombination centers as Cr^{3+} from the 304SS substrate where the electrons can be trapped [29]. Thus, the accumulated charge is higher in this material than the 0.03B-TiO_2/3RGO/Ti composite film. This confirms the high resistivity in the 0.2B-TiO_2/3RGO/304SS composite film, decreasing the electron transport and its PEC performance.

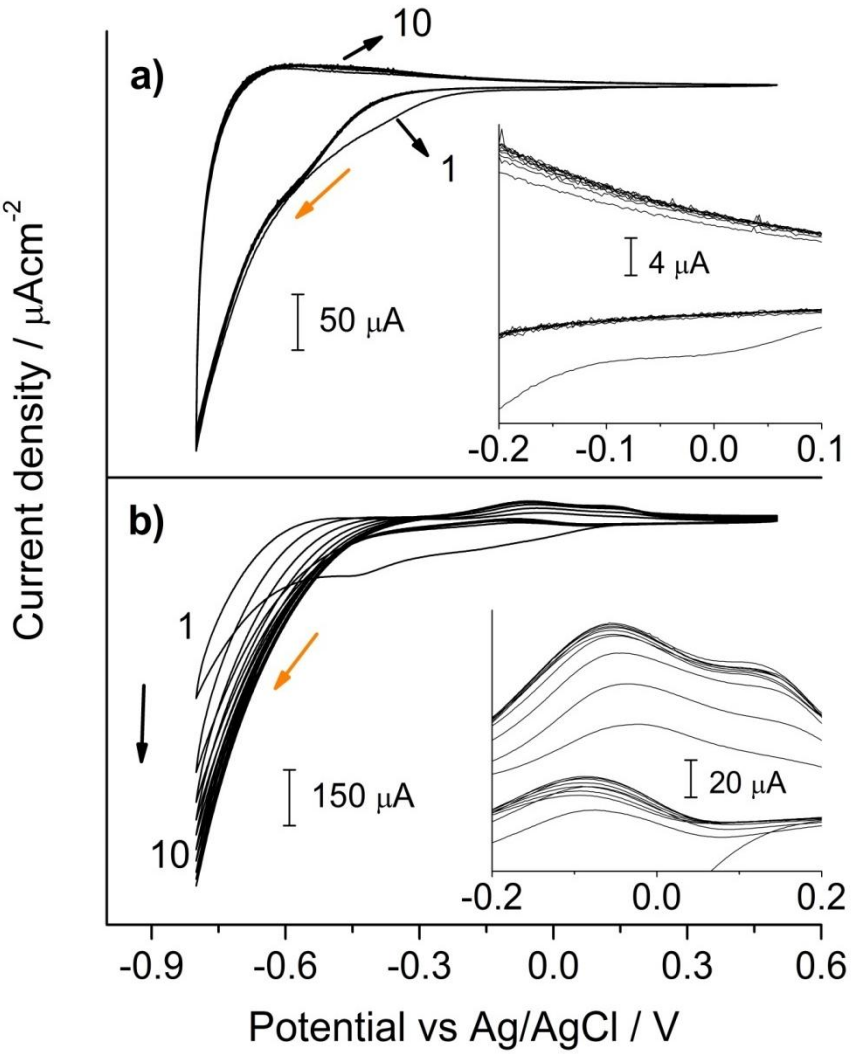

Fig.8. Cyclic voltammograms (10 mVs^{-1}, 10 cycles) obtained in cathodic direction in 0.1 M $HClO_4$for the a) 0.03B-TiO_2/3RGO/Ti and b) 0.03B-TiO_2/3RGO/304SS composite film under the dark.

Figure 9 exhibits the photocurrent generated by the composite films in function on the time by applying an anodic potential of 0.85 V, in 1 mM phenol + 0.1 M $HClO_4$. These measurements were performed with the purpose to observe whether the films characterized by voltammetry are even photoelectrochemically active. For the 0.03B-TiO_2/3RGO/Ti composite film (Figure 9a), the current holds at a constant value in the dark. When the light is ON, the photocurrent is rapidly increased to

reach a steady value. When the light is OFF, the photocurrent decreases and fell back to the initial value [32]. After four ON/OFF light cycles, the film is even photoactive, exhibiting the same behavior. This indicates that the composite film surface is not passivated after the oxidation process, allowing a prolonged electron/hole pair photogeneration [33, 35]. Thus, the phenol oxidation through a photoelectrocatalytic process can be suggested. In the case of 0.03B-TiO_2/3RGO/304SS composite film (Figure 9b), the photocurrent is not increased when the light is ON applying the same potential of 0.85 V which means that its surface is passivated after the oxidation process, inhibiting the electron/hole pair photogeneration. Therefore, the PEC performance of this material is diminished.

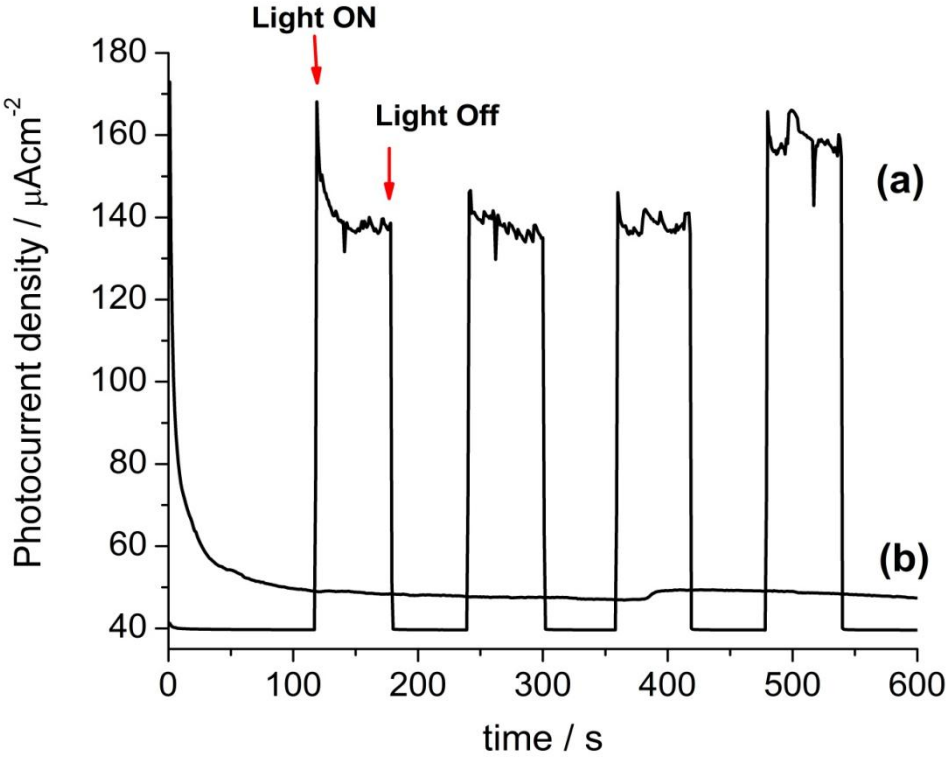

Fig.9. Photocurrent transients (four ON/OFF light cycles under 0.85 V) obtained in 0.1 M HClO4 in presence of 1 mM phenol for the a) 0.03B-TiO2/3RGO/Ti and b) 0.03B-TiO2/3RGO/304SS composite films.

On the other hand, to confirm the photoelectrocatalytic effect in the same 0.03B-TiO_2/3RGO/Ti composite film for the phenol oxidation, the anodic bias potential is changed to observe the generated photocurrent (Figure 10). When the potential is increased, a high generated photocurrent is obtained during the measurements, implying that the electron/hole pair separation is promoted, transporting more electrons to the current collector [32]. The 0.03B-TiO_2/3RGO/Ti composite film is photoelectrochemically active during a prolonged time carrying out the photoelectrocatalytic phenol oxidation.

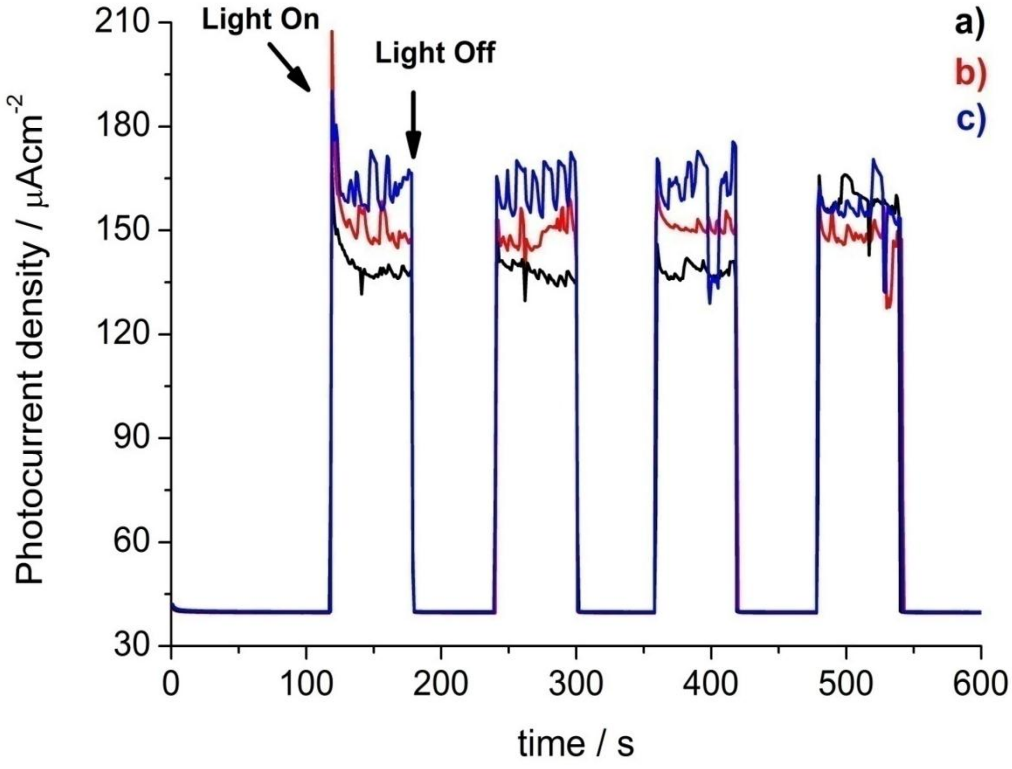

Fig.10. Photocurrent transients (four ON/OFF light cycles) obtained in 0.1 M $HClO_4$ in presence of 1 mM phenol for the 0.03B-TiO_2/3RGO/Ti composite films under a) 0.85 V, b) 1.05 V and c) 1.25 V.

3.3.5 Mott-Schottky plots

Figures 11 and 12 show the Mott-Schottky plots of the 0.03B-TiO_2/3RGO films deposited on 304SS and Ti substrate respectively, obtained in 0.1 M $HClO_4$ in dark conditions. When a semiconductor contacts an electrolytic solution containing redox couples, the charge transference between the semiconductor and the solution is established until an electrochemical equilibrium is reached [39]. The charge excess in the semiconductor is distributed in the space charge layer, which is compensated with by the opposite charges induced in the solution within a localized layer known as the Helmholtz layer. When the space charge layer shows a depletion layer, the relation of the capacitance and the potential obeys the Mott-Schottky equation.

$$\frac{1}{C_{sc}^2} = \frac{2}{\varepsilon\varepsilon_0 qN}\left(V - V_{fb} - \frac{kT}{q}\right) \qquad (2)$$

where, N is the donor or acceptor density, ε the relative dielectric constant of the film (TiO_2, ε = 38), ε_0 the vacuum permittivity, q the elementary charge (+e for electrons, and -e for holes), k the Boltzman constant, T the absolute temperature and V_{fb} the flat-band potential [39] From eq. 2, it can be observed that the C_{sc}^{-2} displays a linear relationship with the applied potential (V), which the Mott-Schottky plots shows a straight line. If the slope of the straight line is positive, it is associated to an n-type semiconductor; if the slope is negative, the result is attributed to a p-type semiconductor [40]. The donor or acceptor density N can be determinated from the slope of the straight line, and the flat-band potential V_{fb} can be estimated from the intercept of the straight line on the potential axis [39, 40]. In this work, the donor/acceptor density and the flat-band potentials were measured at a constant frequency of 7 kHz. For the 0.03B-TiO_2/3RGO/304SS composite film (Figure 11), the plot exhibits three potential regions (I, II and III), with different capacitance responses. The region I is associated to the formation of Cr_2O_3 while the region III is attributed to the formation of Fe_2O_3. Both oxides are present in the

304SS substrate [39]. Ambat et al [10] reported the contributions of Cr_2O_3 in the region I, Fe_2O_3 and TiO_2 in the region III in a TiO_2 film deposited on a 316LSS plate. As the 0.03B-TiO_2/3RGO composite film is also a n-type semiconductor, it contributes to the signal obtained in the region III. The region II is localized near to the flat-band potential [41].

It can be observed that the donor (N_d) and acceptor (N_a) densities determinated from the plots (Table 5) for the 0.03B-TiO_2/3RGO/304SS composite film present an increase compared with the TiO_2/304SS and 0.03B-TiO_2/304SS films (plots not shown). After boron doping, the Ti^{3+} species are formed in the TiO_2 lattice, increasing the donor states in the 0.03B-TiO_2/304SS film and 0.03B-TiO_2/3RGO/304SS composite film. This is confirmed by XPS analysis. The Ti^{2+} species formed during the thermal treatment are also contributes as donor states in the 0.03B-TiO_2/3RGO/304SS composite film. On the other hand, RGO also contributes to the semiconducting properties of the composite film due to it can provide donor and acceptor states. This was reported by Pelc et al [42]. Thus, the donor and acceptor densities for the 0.03B-TiO_2/3RGO/304SS composite film are increased even more. The donor and acceptor states in this composite film are also associated to the Fe^{2+} and Fe^{3+} species in the Fe_2O_3 [43], and the Cr^{3+} recombination centers in the Cr_2O_3 [29], respectively, from the 304SS substrate. The flat-band potential of the n-type semiconductor contribution for the 0.03B-TiO_2/3RGO/304SS composite film shifts anodically with respect to TiO_2/304SS and 0.03B-TiO_2/304SS films, which confirms the increase in the majority charge carriers (electrons) in the composite film. This implies that a potential above the flat-band potential can be applied to extend the depletion layer within the space charge layer of the composite film [39, 41].

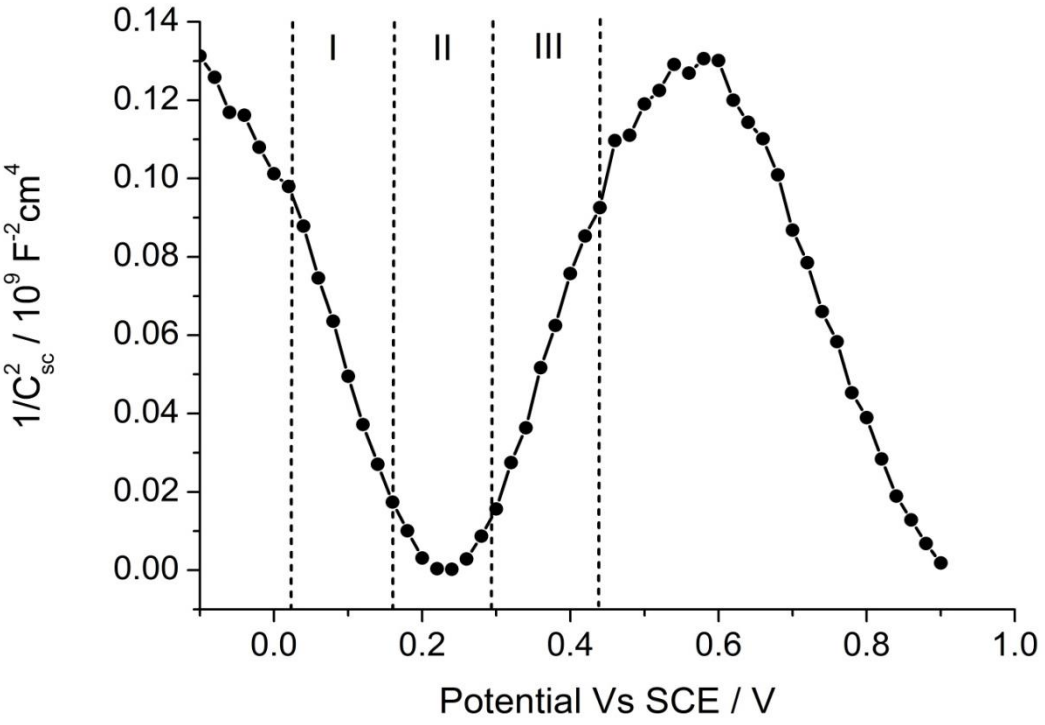

Fig.11. Mott-Schottky plots (from 0.9 V to -0.1 V at 7KHz) obtained in 0.1 M $HClO_4$for the 0.03B-TiO_2/3RGO/304SS composite film under the dark.

Table5. Mott-Schottky parameters for the films deposited on 304SS

Composite film	N_d 10^{21} / cm^{-3}	N_a 10^{21} / cm^{-3}	V_{fb} n-type semiconductor (V vs SCE)	V_{fb} p-type semiconductor (V vs SCE)
TiO_2	1.07	-	0.01	-
0.03B-TiO_2	10.6	9.5	0.26	0.18
0.03B-TiO_2/3RGO	10.8	10.6	0.28	0.19

For the 0.03B-TiO_2/3RGO/Ti composite film (Figure 12), the Mott-Schottky plot shows two potential regions I and II. The region I is localized near to the flat-band potential, while the region II indicates the presence of a n-type semiconductor in the composite film [33]. Compared with the TiO_2/Ti and 0.03B-TiO_2/Ti films (plots not shown) the donor density (Table 6) is increased in a low proportion after boron

doping, which confirms that the three films shows the same donor states content. These states are associated to the Ti^{3+} donor species determinated by XPS. The Ti^{2+} species formed after boron doping also contributes as donor states in the 0.03B-TiO_2/3RGO/Ti composite film. However, after the RGO incorporation, the donor density increases about twice with respect the 0.03B-TiO_2/Ti film. This indicates the incorporation of donor states by RGO, similar to the 0.03B-TiO_2/3RGO/304SS composite film. The absence of a p-type semiconductor contribution implies that in the potential range established in the measurement, the n-type semiconductor is the most important contribution in the semiconducting properties of the 0.03B-TiO_2/3RGO/Ti composite film [35].

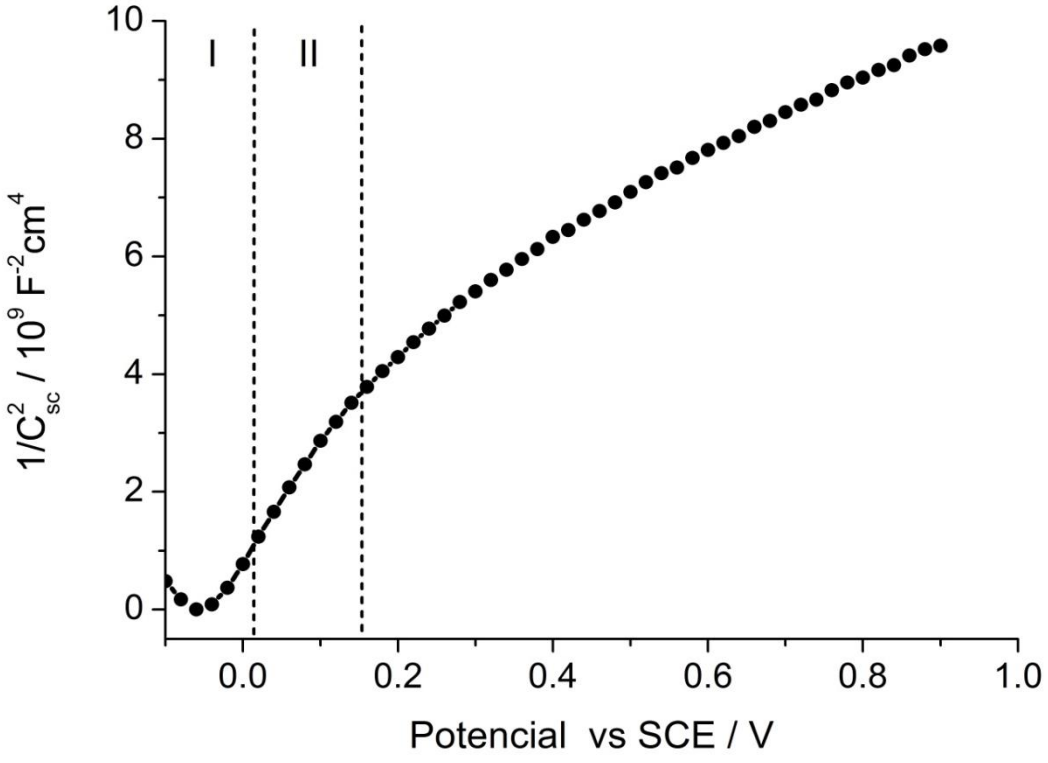

Fig.12. Mott-Schottky plots (from 0.9 V to -0.1 V at 7KHz) obtained in 0.1 M HClO4for the 0.03B-TiO2/3RGO/304SS composite film under the dark.

Table6. Mott-Schottky parameters for the films deposited on Ti

Composite film	N_d 10^{20} / cm^{-3}	V_{fb} n-type semiconductor (V vs SCE)
TiO_2	0.12	-0.069
0.03B-TiO_2	0.13	-0.061
0.03B-TiO_2/3RGO	0.29	-0.036

The donor density provided by RGO can be estimated by subtracting the donor density calculated in the 0.03B-TiO_2/3RGO and the 0.03B-TiO_2 films deposited in both substrates. The donor density of RGO in the film deposited on 304SS is the 2.0 x 10^{20} cm^{-3}, while for the film on Ti is the 1.6 x 10^{20} cm^{-3}. This confirms that RGO was approximately incorporated in a same amount during the films preparation.

The flat-band potential of the 0.03B-TiO_2/3RGO/Ti composite film is also anodically shifted, displacing the depletion layer to more positive potentials similar to 0.03B-TiO_2/3RGO/304SS composite film, but it can be observed that the depletion layer within the space charge layer of the 0.03B-TiO_2/3RGO/Ti composite film is extended with a lower potential value above the flat-band potential compared with the 0.03B-TiO_2/3RGO/304SS composite film [44]. This indicates that the minority charge carrier accumulation (holes) is easily reached to less positive potential compared with the 0.03B-TiO_2/3RGO/304SS film [41].

On the other hand, the donor states density of the 0.03B-TiO_2/3RGO/304SS composite film is one magnitude order higher than the 0.03B-TiO_2/3RGO/Ti composite film due to this former material is also provided by donor states in the Fe_2O_3 from the 304SS [44]. However, the acceptor states contribution is not present inthe0.03B-TiO_2/3RGO/Ti composite film [33,35,45]. The 0.03B-TiO_2/3RGO/304SS composite film exhibits a high acceptor states density which induces the high electron trapping [29], restraining the electron transport and the charge carrier separation in the composite film when it is illuminated. The 0.03B-

TiO_2/3RGO/Ti composite film exhibits a low electron trapping due to it not presents ahigh acceptor states contribution, improving the electron transport within the film, which facilitates the electron/hole pair separation [35]. Hence, the film deposited on Ti is more photoelectrochemically active to carry out the phenol oxidation with a high effectiveness. These observations are in a good accordance with the voltammetry and photocurrent transients results described above. It can be mentioned that the semiconducting properties of the composite films defines their PEC performance in the pollutants oxidation. This is also reported by Eli et al [45] describing the increase in the photoelectrochemical properties for the methyl orange oxidation with the increase of the donor states in the TiO_2 films.

3.3.6 Photoelectrochemical phenol oxidation

Figure 13 and 14 shows the PEC activity of the 0.03B-TiO_2/3RGO/304SSand the 0.03B-TiO_2/3RGO/Ti composite films during the phenol oxidation under UV-Vis light illumination. Direct photolysis (DP), photocatalysis (PC) and electrochemical measurements (EC) were studied in each composite film for comparative purposes. The change of the absorbance (A/A_0) for phenol at 270 nm was analyzed every 30 minutes. The photoelectrochemical process (PEC) was carried out under an applied potential of 0.85 V, to observe the photoelectrocatalytic activity of the films. The UV-Vis light produces direct photolysis (DP) to the organic compound, indicating that phenol is unstable under this irradiation [48]. After 3 h of illumination, phenol was oxidized in 12%. For the 0.03B-TiO_2/3RGO/304SS composite film (Figure 13), in the EC process, the phenol was oxidized in 13 % [14, 15] while the phenol was oxidized in 16% after the PC process, implying a high electron/hole pair recombination in the composite film, hindering the oxidation process. In the PEC process, the electron/hole pair photogeneration is enhanced compared with respect to the PC process during the first 60 min, but after this time the oxidized phenol ratio holds constant as consequence of the inhibition of charge

carrier separation, hindering the oxidation process. During this process, the phenol was oxidized in 17%.

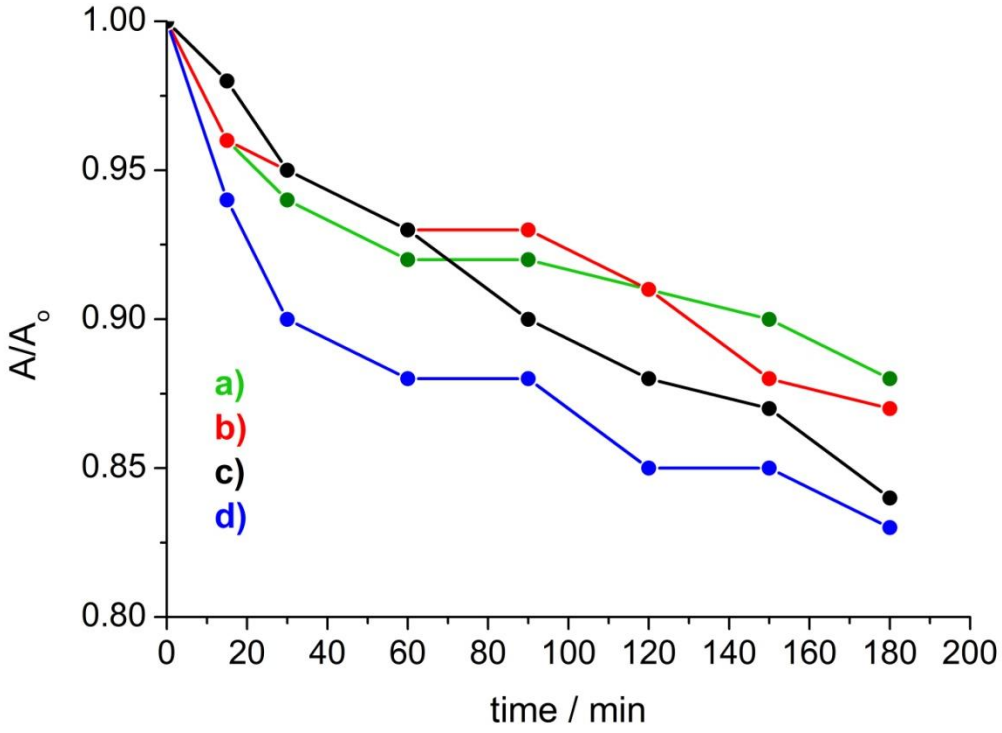

Fig.13.phenol oxidation (1 mM, 40 mL) as function of reaction time in the a) DP, b) EC, c) PC and d) PEC processes using the 0.03B-TiO2/3RGO/304SS composite film.

For the 0.03B-TiO_2/3RGO/Ti composite film (Figure 14), the EC, PC and PEC processes carried out the phenol oxidation in 11%, 20% and 28 % respectively [33, 36]. Under dark conditions, the composite film presents a low electrochemical activity, similar to the 0.03B-TiO_2/3RGO/304SS composite film. In the PC process, the electron/hole pair photogeneration is highly facilitated due to the low electron trapping, promoting the holes accumulation in the semiconductor to oxide phenol [36]. However, The PEC process decreases the electron/hole pair recombination exhibited in the PC process, increasing the holes accumulation in the composite film to improve the oxidation process [45].

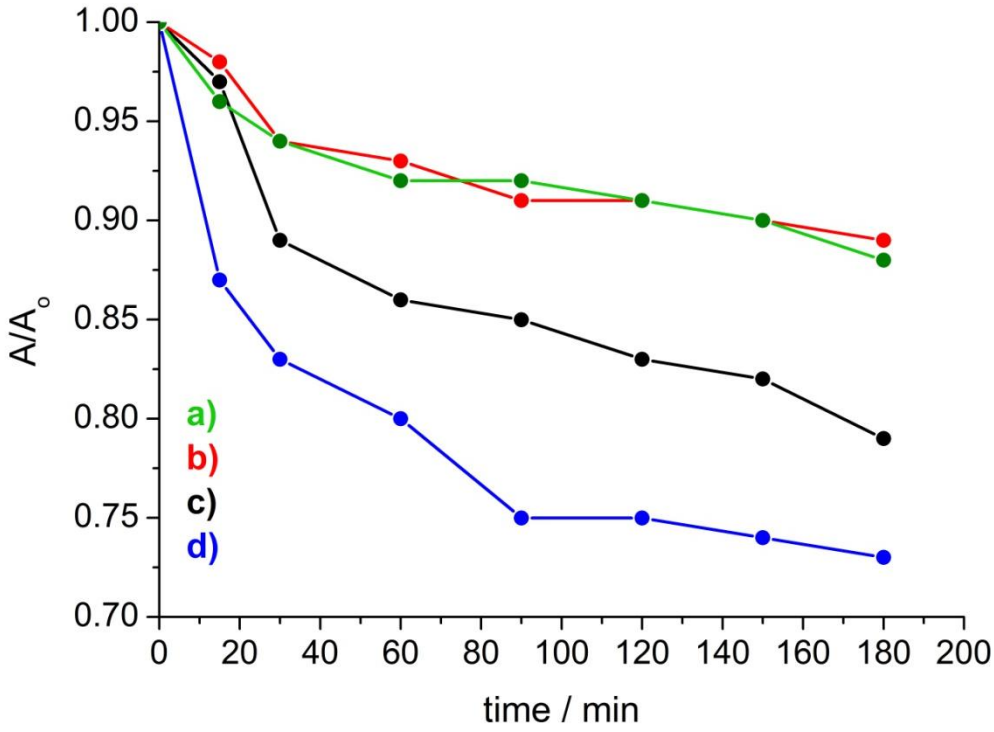

Fig.14. phenol oxidation (1 mM, 40 mL) as function of reaction time in the a) DP, b) EC, c) PC and d) PEC processes using the 0.03B-TiO_2/3RGO/Ti composite film.

In order to observe the PEC activity of the composite filmsunder an irradiation of lower energy, the composite films were illuminated with visible light and the geometry area was increased to 3.0 cm^2 to maximize the light absorption. Figure 15 shows that the phenol oxidation in the 0.03B-TiO_2/3RGO/304SS composite film is carried out in 24 %(Figure 15a) while that in the 0.03B-TiO_2/3RGO/Ti composite film, phenol was oxidized in 51% (Figure15b). Hence, the 0.03B-TiO_2/3RGO/Ti composite film displays a high PEC activity for the phenol oxidation about twice compared with the 0.03B-TiO_2/3RGO/304SS composite film.

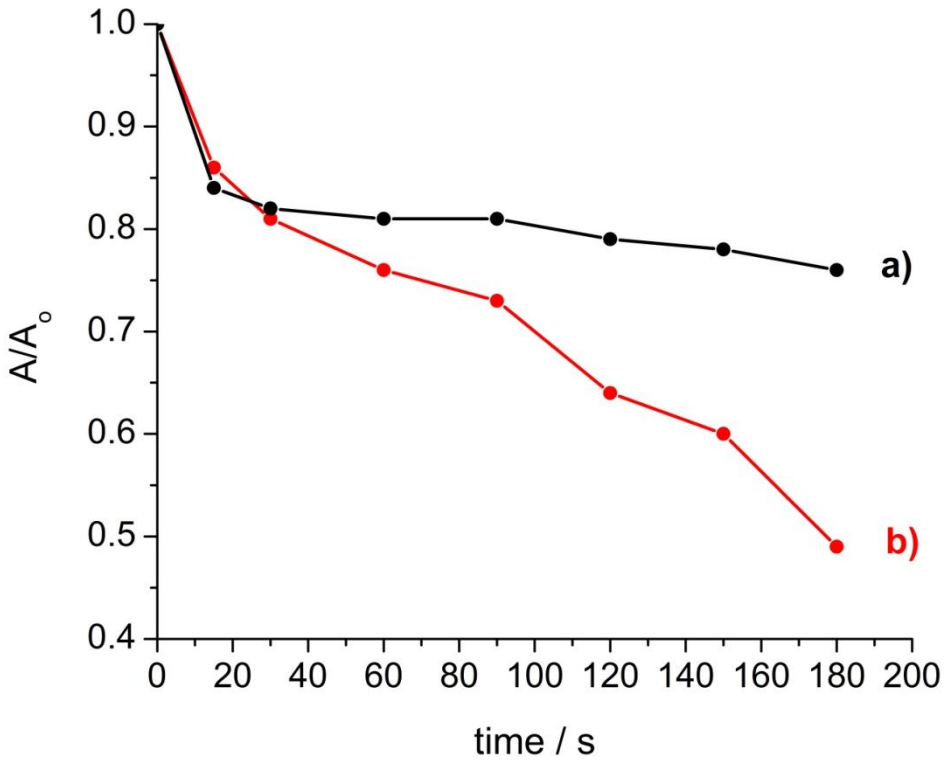

Fig.15. PEC phenol oxidation (1 mM, 40 mL) as function of reaction time using the a) 0.03B-TiO_2/3RGO/304SS and b) the 0.03B-TiO_2/3RGO/Ti composite films.

3.4 Conclusions

The 0.03B-TiO_2/3RGO composite films deposited on 304SS and Ti substrates were successfully prepared by sol-gel method and dip-coating technique. The 0.03B-TiO_2/3RGO/Ti composite film exhibits the best photoelectrochemical properties to oxide phenol due to the formation of a high Ti^{3+} donor states content in the composite film during the thermal treatment, promoting the electron/hole pair separation and the holes accumulation in the semiconductor. Thus, the photoelectrocatalytic phenol oxidation is carried out in the composite film which shows to be photoelectrochemically active during a prolonged time. The 0.03B-TiO_2/3RGO/304SS composite film shows a low photoelectrochemical performance

due to the high resistive features of 304SS, hindering the electron transport within the film, which restrains the charge carrier separation. Thus, the holes accumulation in the material decreases. On the other hand, Although the 0.03B-TiO_2/3RGO/304SS composite film presents higher donor density due to the two kinds of n-type semiconductors as $Fe_2O_3$and the 0.03B-TiO_2/3RGO composite film, it also shows a high acceptor states density from the Cr_2O_3 p-type semiconductor, which confirms a high the electron trapping implying a low electron/hole pair separation. Acceptor states are not presented in the 0.03B-TiO_2/3RGO/Ti composite film, diminishing the electron trapping, which facilities the photogenerated electron transport to the current collector. Hence, this composite film exhibits a PEC activity about twice compared the 0.03B-TiO_2/3RGO/304SS composite film in the oxidation process.

References

[1] A. Zaleska, Doped-TiO_2: A Review, Recent Pat. Eng., 2 (2008) 157-164.

[2] Q. Ling, J. Sun, Q. Zhou, Preparation and characterization of visible-light-driven titaniaphotocatalyst co-doped with boron and nitrogen. Appl. Surf. Sci., 254 (2008) 3236–3241.

[3] A. Zaleska, E. Grabowska, J. W. Sobczak, M. Gazda, J. Hupka, Photocatalytic activity of boron-modified TiO2under visible light: The effect ofboron content, calcination temperature and TiO2matrixAppl. Catal. B, 89 (2009) 469–475.

[4] J. Yu, X. Zhao, Effect of substrates on the photocatalytic activity of nanometer TiO_2 thin films Mater. Res. Bull., 35 (2000) 1293–1301.

[5] D. Wang, X. Li, J. Chen, X. Tao, Enhanced photoelectrocatalytic activity of reduced graphene oxide/TiO_2 composite films for dye degradation. Chem. Eng. J., 198–199 (2012) 547–554.

[6] Fan, T. Peng, B. Chai, J. Chen, K. Dai, Fabrication and photoelectrochemical properties of TiO2films on Ti substrate for flexible dye-sensitized solar cells. Electrochim. Acta, 55 (2010) 5239–5244.

[7] J. Durantini, P. P. Boix, M. Gervaldo, G. M. Morales, L. Otero, J. Bisquert, E. M. Barea, Photocurrent enhancement in dye-sensitized photovoltaic devices with titania–graphene composite electrodes. J. Electroanal. Chem., 683 (2012) 43–46.

[8] P. Wang, Y. Ao, C. Wang, J. Hou, J. Qian, Enhanced photoelectrocatalytic activity for dye degradation by graphene–titania composite film electrodes. J. Hazard. Mater., 223–224 (2012) 79–83.

[9] L. Lopez, W. A. Daouda, D. Duttaa, B. C. Panther, T. W. Turney, Effect of substrate on surface morphology and photocatalysis of large-scale TiO_2 films. Appl. Surf. Sci., 265 (2013) 162-168.

[10] S. Daviðsdóttir, S. Canulescu, K. Dirscherl, J. Schou, R. Investigation of photocatalytic activity of titanium dioxide deposited on metallic substrates by DC magnetron sputtering.Ambat, Surf. Coat. Technol., 216 (2013) 35–45.

[11] S. Li, Q. Wang, T. Chen, Z. Zhou, Y. Wang, J. Fu, Study on cerium-doped nano-TiO_2coatings forcorrosion protection of 316 L stainless steel. *Nanoscale Res. Lett., 7 (2012) 1–9.*

[12] N. Barati, M.A. FaghihiSani, H. Ghasemi, Z. Sadeghian, S.M.M. Mirhoseini, Preparation of uniform TiO_2 nanostructure film on 316L stainless steel by sol–gel dip coating. Appl. Surf. Sci., 255 (2009) 8328–8333.

[13] H. M. Soliman, A.F. Waheed, Effect of Differential Thermal Expansion Coefficient on Stress Generated in Coating. J. Mater. Sci. Technol., 15 (1999) 452-462.

[14] L. Bao, R. Xiong, G. Wei, Electrochemical polymerization of phenol on 304 stainless steel anodes and subsequent coating structure analysis. Electrochim. Acta, 55 (2010) 4030–4038.

[15] N. B. Tahar, A. Savall, Electrochemical removal of phenol in alkaline solution. Contribution of the anodic polymerization on different electrode materials.Electrochim. Acta, 54 (2009) 4809–4816.

[16] X. Lu, B. Tian, F. Chen, J. Zhang, Preparation of boron-doped TiO_2films by autoclaved-sol method at low temperature and study on their photocatalytic activity. Thin Solid Films, 519 (2010) 111–116.

[17] J. Ding, Y. Yuan, J. Xu, J. Deng, J. Guo, TiO_2Nanopowder Co-Doped with Iodine and Boron to Enhance Visible-Light Photocatalytic Activity. J. Biomed. Nanotechnol., 5 (2009) 1–7.

[18] N. Lu, X. Quan, J. Y. Li, S. Chen, H. T. Yu, G.H. Fabrication of Boron-Doped TiO_2 Nanotube Array Electrode and Investigation of Its Photoelectrochemical Capability. Chen, J. Phys. Chem., 111 (2007) 11836–11842.

[19]B. Choudhury**,** A. Choudhury, Local structure modification and phase transformation of TiO_2 nanoparticles initiated by oxygen defects, grain size, and annealing temperature. Int. Nano Lett., 3 (2013) 1- 9.

[20] L. C. Chen, Y. C. Ho, W.S. Guo, C.M. Huang, T.C. Pan, Enhanced visible light-induced photoelectrocatalytic degradation of phenol by carbon nanotube-doped TiO_2 electrodes. Electrochem. Acta, 54 (2009) 3884–3891.

[21] X. Zhou, T. Shi, J. Wu, H. Zhou, (0 0 1) Facet-exposed anatase-phase TiO_2 nanotube hybrid reduced graphene oxide composite: Synthesis, characterization and application in photocatalytic degradation. Appl. Surf. Sci., 287 (2013) 359–368.

[22] N.R. Khalid, E. Ahmed, Z. Hong, M. Ahmad, Synthesis and photocatalytic properties of visible light responsive La/TiO_2-graphene composites. Appl. Surf. Sci., 263 (2012) 254–259.

[23] N.R. Khalid, Z. Honga, E. Ahmed, Y. Zhang, H. Chan, M. Ahmad, Synergistic effects of Fe and graphene on photocatalytic activity enhancement of TiO_2 under visible light. Appl. Surf. Sci., 258 (2012) 5827–5834.

[24] G. W. Hwang, W. D. Kim, Y. S. Min, Y. J. Cho, C. S. Hwang, Characteristics of Amorphous $Bi_2Ti_2O_7$ Thin Films Grown by Atomic Layer Deposition for Memory Capacitor Applications. J. Electrochem. Soc., 153 (2006) F20-F26.

[25]P. Acevedo-Peña, L. Lartundo-Rojas, I. González, Effect of water and fluoride content on morphologyand barrier layer properties of TiO_2 nanotubes grown in ethylene glycol-based electrolytes. J. Solid. State Electrochem., 17 (2013) 2939–2947.

[26] C. Di Valentin, G. Pacchioni, Trends in non-metal doping of anatase TiO_2: B, C, N and F. Catal. Today, 206 (2013) 12–18.

[27] C. Lei, H. Zhou, C. Wang, Z. Feng, Self-assembly of ordered mesoporous TiO_2 thin films as photoanodes for cathodic protection of stainless steel. Electrochem. Acta, 87 (2013) 245-249.

[28] G. Yang, Z. Jiang, H. Shi, T. Xiao, Z. Yan, Preparation of highly visible-light active N-doped TiO_2photocatalyst. J. Mater. Chem., 20 (2010) 5301–5309.

[29] E. Cho, H. Kwon, D. D. Macdonald, Photoelectrochemical analysis on the passive film formed on Fe – 20Cr in pH 8.5 buffer solution. Electrochem. Acta, 47 (2002) 1661-1668.

[30] V. V. Panić, S.I. Stevanović, V.B. M. Stanković, B. Ž. Jovanović, B. Ž. Nikolić, Photoelectrochemical properties of sol–gel obtained titanium oxide. J. Serb. Chem. Soc., 73 (2008) 1211–1221.

[31] D. M. Satoca, R. Gómez, Electrochemical Method for Studying the Kinetics of Electron Recombination and Transfer Reactions in Heterogeneous Photocatalysis: The Effect of Fluorination on TiO_2Nanoporous Layers. J. Phys. Chem., 112 (2008) 139-147.

[32] X. Dong, J. Tao, Y. Li, H. Zhou, Enhanced Photoelectrochemical Properties of F-containing TiO2 sphere thin film induced by its novel hierarchical structure. Appl. Surf. Sci. 255 (2009), 7183–7187.

[33] J. Y. Shi,W. H. Leng,W. C. Zhu,J. Q. Zhang, C. N. Cao, Electrochemically Assisted Photocatalytic Oxidation of Nitrite over Cr-Doped TiO_2 under Visible Light. Chem. Eng. Technol., 29 (2006) 146-154.

[34] T. L.Villarreal, Y. Mao, S. S. Wong, R. Gómez, Photoelectrochemicalbehaviour of anatasenanoporous films: effect of the nanoparticle organization. Nanoscale, 2 (2010) 1690–1698.

[35] H. S. Kim, D. T. Nguyenb, E. Shin, J. Lee, S. K. Lee, K. Ahn, S. H. Kang, Bifunctional doping effect on the TiO_2 nanowires for photoelectrochemical water splitting. Electrochim. Acta, 114 (2013) 159– 164.

[36] Z. Zainal, C. Y. Lee, A. Kassim, M. Z. Hussein, N. A. Yusof, Photoelectrochemical Degradation of Methyl Orange Using TiO_2 /Ti Films Prepared via Sol-Gel Technique. ActaChim. Slov., 54 (2007) 166–174.

[37] D. M. Satoca, T. L. Villarreal, R. Gómez, Effect of Surface Fluorination on the Electrochemical and Photoelectrocatalytic Properties of Nanoporous Titanium Dioxide Electrodes. Langmuir, 27 (2011) 15312–15321.

[38] A. Kocijan, R. Donik, M. Jenko, the electrochemical study of duplex stainless steel in chloride solutions. Mater. Technol., 43 (2009) 39–42.

[39] H. Ge, G. Zhou, W. Wu, Passivation model of 316 stainless steel in simulated cooling water and the effect of sulfide on the passive film. Appl. Surf. Sci., 211 (2003) 321–334.

[40] J. Liu, Y. Duan, X. Zhou, Y. Lin, Influence of $V_B$group doped TiO_2 on photovoltaic performance of dye-sensitized solar cells. Appl. Surf. Sci., 277 (2013) 231–236.

[41] Z. Feng, X. Cheng, C. Dong, L. Xu, X. Li, Passivity of 316L stainless steel in borate buffer solution studied by Mott–Schottky analysis, atomic absorption spectrometry and X-ray photoelectron spectroscopy. Corros. Sci., 52 (2010) 3646–3653.

[42] M. Pelc, W. Jaskólski, A. Ayuela, L. Chico, Octagonal Defects as the Source of Gap States in Graphene Semiconducting Structures. Acta Phys. Pol. A, 124 (2013) 777-780.

[43]M. Barroso, S. R. Pendlebury, A. J. Cowanand, J. R. Durrant, Charge carrier trapping, recombination and transfer in hematite (α-Fe2O3) water splitting photoanodes. Chem. Sci., 4 (2013) 2724–2734.

[44] N.E. Hakiki, M.F. Montemor, M.G.S. Ferreira, M. da Cunha Belo, Semiconducting properties of thermally grown oxide films on AISI 304 stainless steel. Corros. Sci., 42 (2000) 687-702.

[45] N. Baram, Y. E. El, Electrochemical Impedance Spectroscopy of Porous TiO_2 for Photocatalytic Applications. J. Phys. Chem., 114 (2010) 9781–9790.

[46] V. A. Svetlichnyi, O. N. Chaikovskaya, O. K. Bazyl', R. T. Kuznetsova, I. V. Sokolova, T. N. Kopylova, Yu. P. Meshalkin, Photolysis of Phenol and para-Chlorophenol by UV Laser Excitation. High Energ. Chem., 4 (2001) 258-264.

GENERAL CONCLUSION

The B-TiO_2/RGO composite films prepared by the sol-gel dip coating technique exhibit high PEC properties in the phenol oxidation, being 0.03B-TiO_2/3RGO, the composite film that generates the highest photocurrent in this process, which is 30 times compared with TiO_2. Due to the RGO acts as an efficient acceptor and transporter of electrons, the electron transport within the film is enhanced, facilitating the electron/hole pair separation. Thus, the generated photocurrent is increased. However, the photocurrent shows a little decrease as consequence of the resistive features of the 304SS where the film is deposited, which hinder the electron transport through TiO_2 film-current collector interfase. The 0.03B-TiO_2/3RGO deposited on Ti, present a higher generated photocurrent which is 3.2 times compared with the film deposited on 304SS. This increase in the photoresponse is caused by the enhanced electron transport through the current collector composed by this metal, which not display acceptor states compared with 304SS, decreasing the electron trapping in the deposited film. Hence, the photogenerated electron transport is facilitated, leaving more holes accumulated in the film to carry out the PEC oxidation process.

BIBLIOGRAPHY

[1] A. Zaleska, E. Grabowska, J. W. Sobczak, M. Gazda, J. Hupka, Photocatalytic activity of boron-modified TiO_2 under visible light: The effect of boron content, calcination temperature and TiO_2 matrix Appl. Catal., B. 89 (2009) 469–475.

[2] A. Zaleska, Doped-TiO2: A Review, Recent Pat. Eng., 2 (2008) 157-164.

[3] B. Choudhury, A. Choudhury, Local structure modification and phasetransformation of TiO_2 nanoparticles initiated by oxygen defects, grain size, andannealing temperature. Int. Nano Lett. 3 (2013) 1- 9.

[4] C. Di Valentin, G. Pacchioni, Trends in non -metal doping of anatase TiO2: B, C, N and F. Catal. Today 206 (2013) 12–18.

[5] C. Lei, H. Zhou, C. Wang, Z. Feng, Self-assembly of ordered mesoporous TiO_2 thin films as photoanodes for cathodic protection of stainless steel. Electrochem. Acta, 87 (2013) 245-249.

[6] D. Li, M. B. Muller, S. Gilje, R. B. Kanerand, G. G. Wallace, Processable aqueous dispersions ofgraphenenanosheets. Nat. Biotechnol. 3 (2008) 101 – 105

[7] D. Wang, X. Li, J. Chen, X. Tao, Enhanced photoelectrocatalytic activity of reduced graphene oxide/TiO_2 composite films for dye degradation. Chem. Eng. J., 198–199 (2012) 547–554.

[8] Fan, T. Peng, B. Chai, J. Chen, K. Dai, Fabrication and photoelectrochemical properties of TiO2films on Ti substrate for flexible dye-sensitized solar cells. Electrochim. Acta, 55 (2010) 5239–5244.

[9] G. Goodlet, S. Faty, S. Cardoso, P.P. Freitas, A.M.P. Simoes, M.G.S. Ferreira, M. Da Cunha Belo, The electronic properties of sputtered chromium and iron oxide films. Corros. Sci. 46 (2004) 1479–1499.

[10] G. Li, T. Wang, Y. Zhu, S. Zhang, C. Mao, J. Wu, B. Jin, Y. Tian, Preparation and photoelectrochemical performance of Ag/graphene/TiO_2 composite film. Appl. Surf. Sci. 257 (2011) 6568–6572.

[11] G. Liu, X. Wang, L. Wang, Z. Chen, F. Li, G. Qing (Max) Lu, H. M. Cheng, Drastically enhanced photocatalytic activity in nitrogen doped mesoporous TiO_2 with abundant surface states. J. Colloid Interf. Sci. 334 (2009) 171–175.

[12] H. Ge, G. Zhou, W. Wu, Passivation model of 316 stainless steel in simulated cooling water and the effect of sulfide on the passive film. Appl. Surf. Sci., 211 (2003) 321–334.

[13] H. M. Soliman, A.F. Waheed, Effect of Differential Thermal Expansion Coefficient on Stress Generated in Coating. J. Mater. Sci. Technol., 15 (1999) 452-462.

[14] H. S. Kim, D. T. Nguyenb, E. Shin, J. Lee, S. K. Lee, K. Ahn, S. H. Kang, Bifunctional doping effect on the TiO_2 nanowires for photoelectrochemical water splitting. Electrochim. Acta, 114 (2013) 159– 164.

[15] J. Ding, Y. Yuan, J. Xu, J. Deng, J. Guo, TiO_2 Nanopowder Co-Doped with Iodine and Boron toEnhance Visible-Light Photocatalytic Activity, J. Biomed.Nanotechnol. 5 (2009) 1–7.

[16] J. Durantini, P. P. Boix, M. Gervaldo, G. M. Morales, L. Oter o, J. Bisquert, E. M. Barea, Photocurrent enhancement in dye-sensitized photovoltaic devices with titania–graphene composite electrodes. J. Electroanal. Chem. 683 (2012) 43–46.

[17] K. Krishnamoorthy, M. Veerapandian, G. Kimand, S. J. Kim, A One Step Hydrothermal Approach for the Improved Synthesis of GrapheneNanosheets. Curr. Nanosci. 8 (2012) 934-938.

[18] L. Bao, R. Xiong, G. Wei, Electrochemical polymerization of phenol on 304 stainless steel anodes and subsequent coating structure analysis. Electrochim. Acta 55 (2010) 4030–4038.

[19] L. C. Chen, Y. C. Ho, W.S. Guo, C.M. Huang, T.C. Pan, Enhanced visible light-induced photoelectrocatalytic degradation of phenol by carbon nanotube - doped TiO2 electrodes. Electrochem. Acta, 54 (2009) 3884–3891.

[20] L. Lopez, W. A. Daouda, D. Duttaa, B. C. Panther, T. W. Turney, Effect of substrate on surface morphology and photocatalysis of large-scale TiO_2 films. Appl. Surf. Sci. 265 (2013) 162-168.

[21] Lu, H. Zhao, J. Li, X. Quan, S. Chen, Characterization of boron-doped TiO_2 nanotube arrays prepared by electrochemical method and its visible light activity. Sep. Purif. Technol. 62 (2008) 668–673.

[22] M. Barroso, S. R. Pendlebury, A. J. Cowanand, J. R. Durrant, Charge carrier trapping, recombination and transfer in hematite (α-Fe2O3) water splitting photoanodes. Chem. Sci., 4 (2013) 2724–2734.

[23] M. Pelc, W. Jaskólski, A. Ayuela, L. Chico, Octagonal Defects as the Source of Gap States in Graphene Semiconducting Structures. Acta Phys. Pol. A, 124 (2013) 777-780.

[24] N. Baram, Y. E. El, Electrochemical Impedance Spectroscopy of Porous TiO_2 for Photocatalytic Applications. J. Phys. Chem. 114 (2010) 9781 –9790.

[25] N.E. Hakiki, M.F. Montemor, M.G.S. Ferreira, M. da Cunha Belo, Semiconducting properties of thermally grown oxide films on AISI 304 stainless steel. Corros. Sci., 42 (2000) 687-702.

[26] N.R. Khalid, E. Ahmed, Z. Hong, M. Ahmad, Synthesis and photocatalytic properties of visible light responsive La/TiO_2-graphene composites. Appl. Surf. Sci., 263 (2012) 254–259.

[27] N.R. Khalid, Z. Honga, E. Ahmed, Y. Zhang, H. Chan, M. Ahmad, Synergistic effects of Fe and graphene on photocatalytic activity enhancement of TiO_2 under visible light. Appl. Surf. Sci., 258 (2012) 5827–5834.

[28] P. Wang, Y. Ao, C. Wang, J. Hou, J. Qian, Enhanced photoelectrocat alytic activity for dye degradation by graphene–titania composite film electrodes. J. Hazard. Mater., 223–224 (2012) 79–83.

[29] Q. Ling, J. Sun, Q. Zhou, Preparation and characterization of visible-light-driven titania photocatalyst co-doped with boron and nitrogen. Appl. Surf. Sci., 254 (2008) 3236–3241.

[30] S. Daviðsdóttir, S. Canulescu, K. Dirscherl, J. Schou, R. Investigation of photocatalytic activity of titanium dioxide deposited on metallic substrates by DC magnetron sputtering.Ambat, Surf. Coat. Technol., 216 (2013) 35–45.

[31] T. L.Villarreal, Y. Mao, S. S. Wong, R. Gómez, Photoelectrochemical behaviour of anatase nanoporous films: effect of the nanoparticle organization. Nanoscale, 2 (2010) 1690–1698.

SUPPLEMENTARY MATERIAL – ANEXXES

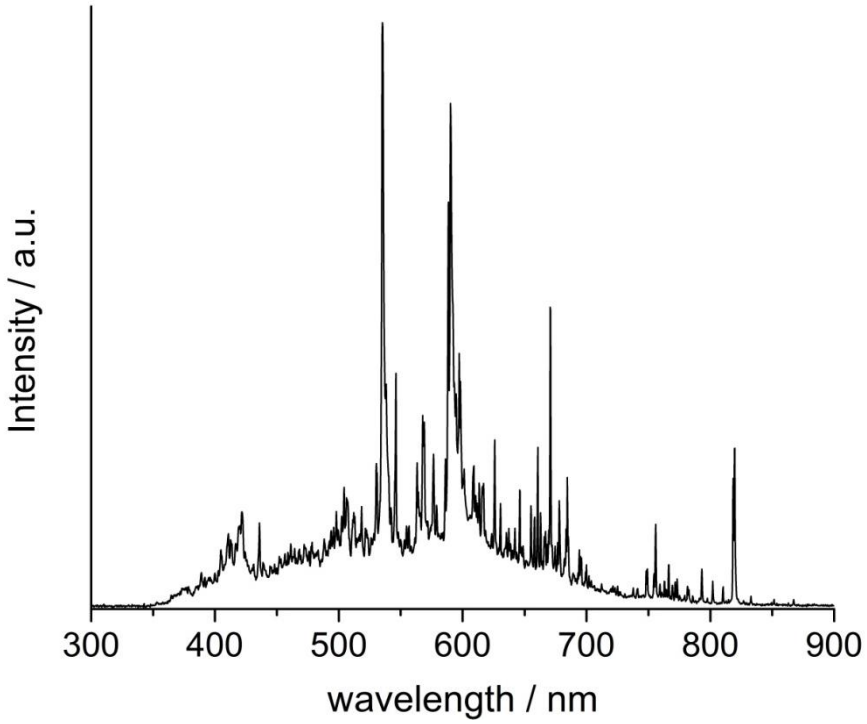

Fig.1S. Emission spectrum of visible light source